2009

Functionally gradient syntactic foams

Kanakaji Chittineni
Louisiana State University and Agricultural and Mechanical College

FUNCTIONALLY GRADIENT SYNTACTIC FOAMS

A Thesis

Submitted to the Graduate Faculty of the
Louisiana State University and
Agricultural and Mechanical College
in partial fulfillment of the
requirements for the degree of
Master of Science

in

The Department of Mechanical Engineering

by
Kanakaji Chittineni
Bachelor of Engineering
Jawaharlal Nehru Technological University, India, 2006
July 2009

ACKNOWLEDGEMENTS

I would like to express sincere gratitude to my major Professor Dr. Eyassu Woldesenbet for his constant motivation, financial support and guidance throughout my research work in Louisiana State University. I also thank him for raising the burning desire on research with his enthusiastic words. Also, I would like to thank the graduate committee members Dr. Guoqiang Li and Dr. Su-Seng Pang for their valuable time to evaluate my thesis document. I am also thankful to my committee members for their thought provoking insights during defense that is deeply instrumental in completion of my thesis.

I would like to thank DOW Chemical Company and 3M for providing epoxy resin and microballoons, respectively and technical information for the experimental study. I sincerely appreciate the help of Dr. Xiaogang Xie, Research Associate, Geology Department for his guidance in obtaining Scanning Electron Microscopy (SEM) images of gradient structures.

I would like to thank and express my sincere gratitude to Dr. Phani Mylavarapu. I can never forget his encouragement and motivation during my initial days of research work. Also, he spent so much time to read my research papers and thesis. I also thank him for his valuable discussions which helped me to complete thesis document so easily. My sincere thanks to Mr. Manu John for his immense support during fabrication and for his valuable advices about research work. A special thanks to Mr. Venkata Sandeep Chakka and Mr. Sameer Leo Peter, for stimulating me towards my goal whenever I lose my enthusiasm.

I would also like to thank my roommates, Mr. Madhav Gullapalli and Mr. Shrvan Kilaru for their continuous backing and encouragement and making my stay in USA as pleasant as possible. I would like to thank my friends in special for their assistance right from my initial days in USA. Without delaying, I would like to thank all my labmates for maintaining fun filled

atmosphere in lab without disturbing its seriousness. Most importantly I can never forget those composite group seminars because that makes me to learn new approaches and techniques of work. Also, I am grateful to my friends back in India for their moral support and help.

Finally and most importantly with a sole heart, I would like to acknowledge my parents, Mr. Srimannarayana Chittineni and Mrs. Rama Devi Chittineni and my brothers, Mr. Sivaji Chittineni and Mr. Rama Krishna Chittineni for their emotional attachment, valuable suggestions and wonderful guidance towards my goals of life. And finally, I would like to thank to all my relatives for their wishes and prayers.

TABLE OF CONTENTS

LIST OF FIGURES

LIST OF TABLES

ABSTRACT

Syntactic foams are comprised of hollow microballoons in matrix systems. The superior mechanical and physical properties of syntactic foams such as light weight, high compressive strength, and low moisture absorption make them attractive materials for structural applications. As these materials are used in high mechanical performance applications, there is a need to achieve both high compressive strength and high energy absorption with minimal or no increase in density. In this study, the effect of gradient configuration of syntactic foams on the energy absorption and compressive strength is studied. Functionally Gradient Syntactic Foams (FGSFs) in five different layer sequencings are fabricated using layer over layer integrated technique called integrated FGSFs (IFGSFs). Each syntactic foam layer in IFGSF is fabricated using one of the four different types of glass microballoons namely, S22, S32, S38 and K46. In the present study, gradient structures are created with the variation of microballoon wall thickness. In order to maintain uniformity in the structure, volume fraction of the microballoons in each layer of IFGSF is maintained constant at 60%. The different layers of IFGSFs are integrated before major solidification takes place. Five different layer sequencing IFGSFs are fabricated to understand the effect of layer sequencing on the compressive properties of gradient structures. IFGSFs have tested for flat-wise and edge-wise compression properties on MTS-810 servo hydraulic machine. Also, flat-wise compression results are compared with adhesively bonded FGSF and found that FGSFs fabricated with layer over layer integrated technique show dramatic improvement in compressive properties. Furthermore, the IFGSF results are compared to one another for understanding the effect of layer sequencing on flat-wise and edge-wise compressive behavior. Layer sequencing effect on crack propagation behavior of IFGSFs is carefully monitored and analyzed with Optical Microscope (OM) and Scanning Electron Microscope

(SEM). In order to understand the dynamic properties of gradient structures, low velocity impact analysis is performed on the IFGSF structures. Impact testing of IFGSFs is conducted at velocities 1 m/s, 2 m/s and 3 m/s on Dynatup 8250 impact testing machine. The initiation energy, propagation energy and maximum load values of IFGSFs are compared to one another to understand the layer sequencing effect on impact properties.

CHAPTER 1. INTRODUCTION

1.1 Composite Materials

1.1.1 Definition

Emerging technology and its requirement for high performance materials are increasing day by day. Improved the performance of material is limited when a material has only one composition. Therefore, new high performance materials can be created by combining two or more conventional materials. These materials which are a combination of multiple constituents are termed as composites. According to ASM Handbook [1], composites can be defined as "a macroscopic combination of two or more distinct material having a recognizable interface between them." Composite materials are flexible materials for multifunctional applications due to their significant properties such as high specific strength, modulus, bending stiffness and chemical resistance.

1.1.2 Basic Constituents of Composites

Composite materials are comprised of two basic constituents namely, matrix and reinforcement. The matrix can be polymer, metal matrix or ceramic based. Polymer matrix materials include thermosets such as epoxy, phenolic and vinyl ester; or thermoplastics such as polyetherketone and polyethersulphone. Metal matrix materials are made by dispersing a reinforcing material into a metal matrix. The matrix used in these metal matrix composites is usually a lighter metal such as Aluminum (Al), Magnesium (Mg), or Titanium (Ti). Polymer matrix composites are used in modern day structural applications due to their significant advantages such as resistance to corrosion, resistance to chemicals, high strength to weight ratio, low thermal and electrical conductivity, and low moisture absorption. The reinforcement can be either continuous or discontinuous phase. Continuous phase of reinforcement include long

fibers. Discontinuous phase of reinforcement include short fibers, whiskers or particles. Reinforcement in composites can also be single phase or multiphase. A multiphase reinforcement can be achieved by using different particles together.

1.1.3 Advantages and Limitations of Composites

1.1.3.1 Advantages

- Higher design flexibility to achieve preferred mechanical and physical properties by varying the constituents.
- High strength to weight ratio and low cost.
- High thermal resistance, low coefficient of moisture absorption, and excellent resistance to chemicals and corrosion

  Due to these advantages, composites are attractive in weight sensitive applications such as aerospace, naval, sports, packaging, and automobile applications

1.1.3.2 Limitations

- Less reliable for new applications, because of the difficulties in design analysis and modeling.
- Not suitable for mass production due to its fabrication difficulties, higher cost of fabrication and repair.

1.1.4 Classification of Composites

Based on the reinforcement, composites are broadly classified into fiber reinforced and particulate reinforced [2].

1.1.4.1 Fiber Reinforced Composites

Fiber Reinforced Polymer (FRP) composites are fabricated by incorporating one or more continuous or discontinuous reinforcing phase of fiber in a continuous matrix phase. The

properties of FRP composites can be varied by varying the arrangement and orientation of the fibers relative to one another, fiber concentration and fiber distribution. These composites are widely used in high performance structural applications due to their significant properties such as high strength and superior blast resistance [3]. Examples of fiber reinforced polymer composites include, glass fiber reinforced polymer composites and carbon fiber reinforced polymer composites etc.

1.1.4.2 Particulate Composites

Particulate composites are fabricated by reinforcing one or more particulate phase in a continuous matrix phase. Size, shape, volume fraction and properties of filler particles affect the properties of particulate composites. Some of the common particle shapes used in particulate composites include spherical, flaky and cubical. Due to the difference in particle shape and size, the surface area could be different for different particles even at same volume fraction. Further the bonding between particle and matrix along with stress concentration factor are dependent on particle aspect ratio. Appropriate selection of particle shape and size is important for producing composites having superior strength, high damage tolerance, excellent wear and chemical resistance. Examples of particulate composites include polymer resin matrix containing aluminum, steel or glass particles. Out of these particulates, hollow glass particulate composites also called as syntactic foams gained significant importance due to their light weight and high specific strength.

1.2 Syntactic Foams

1.2.1 Definition

Syntactic foams are examples of particulate composite materials. According to American Society for Testing and Materials [4], syntactic foam is defined as a “material consisting of

hollow spherical fillers in a resin matrix." The hollow spheres are called microballoons. Syntactic foams possess lower density due to the hollow microballoons incorporated in the matrix as compared to solid particulate composites and fiber reinforced composites. Microballoons used in syntactic foams can be of glass, ceramic, steel and aluminum [5-7] and are available in various sizes [8].

1.2.2 Advantages of Syntactic Foams

Syntactic foam composites are found to possess high specific strength [9] and low thermal conductivity [10]. These composites are used as core materials in sandwich structures for various weight sensitive applications due to their significant advantages such as high specific compressive strength, high damage tolerance, thermal and electrical insulation and excellent damping properties[11]. The multi-functionality of syntactic foams is due to their wide range of mechanical properties coupled with vibration damping characteristics and ability to be fabricated in functionally graded form.

1.2.3 Applications of Syntactic Foams

Syntactic foams are initially developed in 1960s as buoyancy aid materials for deep sea applications [12]. Later, syntactic foams have gained much more importance as aircraft, spacecraft and naval structural applications [13-15]. Depending upon the application, the matrix material, microballoons, volume fraction of microballoons, and density of microballoons in syntactic foams can be varied. Studies have shown that the density of syntactic foams can be varied in two different ways [16]. The density of syntactic foam can be varied either by changing the volume fraction of microballoons or by changing the density of microballoons. The second method gives greater design flexibility, as any change in properties of syntactic foam can be related to the radius ratio (η) of microballoons. Radius ratio (η) is defined as the ratio of

inner radius (r_i) to outer radius (r_0) of microballoons as shown in Eq. (1). The schematic representation of individual microballoon is shown in Figure 1. The difference between outer radius (r_0) and inner radius (r_i) is termed as wall thickness. Density and strength of microballoons is inversely proportional to the radius ratio. Lower wall thickness, higher internal radius microballoons gives lower density and lower strength syntactic foams. In contrast, higher density microballoons impart higher compressive strength and lower fracture strain to syntactic foams [17]. Considering the applications of syntactic foams in naval and aerospace structural applications, the effect of the internal radius on the mechanical properties of syntactic foams was widely studied [9, 15, 28].

$$\eta = \frac{r_i}{r_o} \tag{1}$$

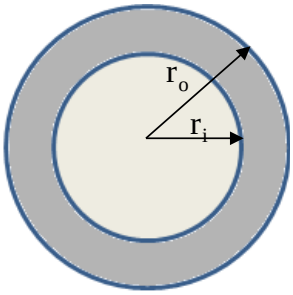

Figure 1 Schematic representation of individual microballoon

1.2.4 Structure of Syntactic Foam

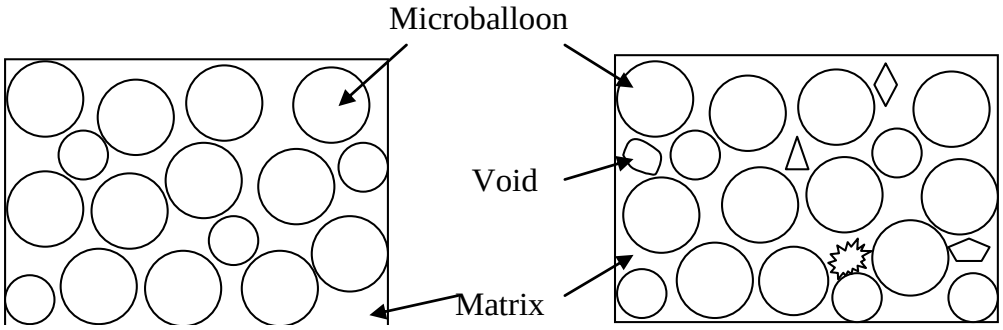

Figure 2 Schematic representation of two phased and three phased syntactic foams

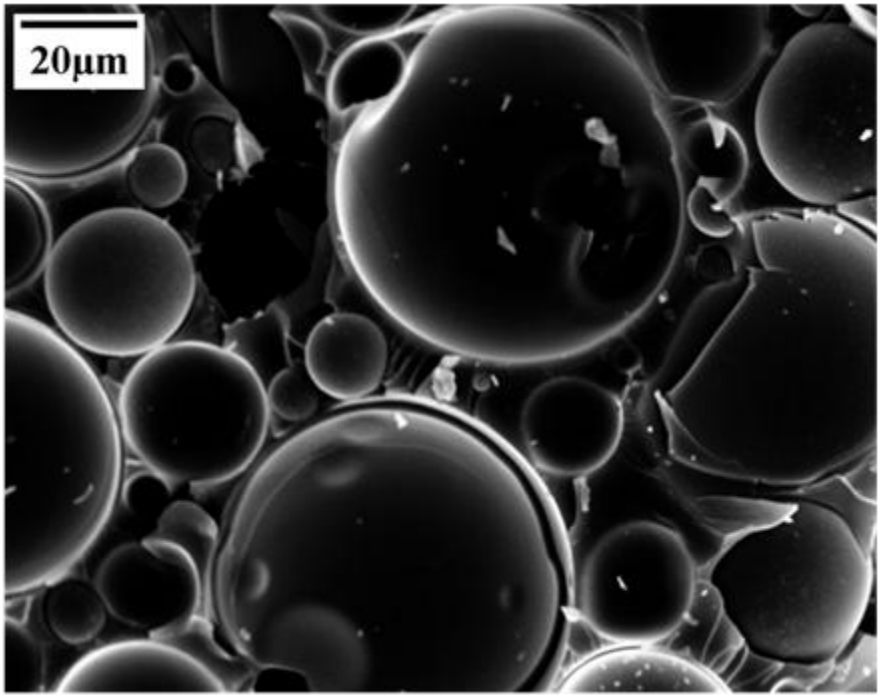

Figure 3 Micro structure of glass microballoons syntactic foam at cut surface

Syntactic foams are usually a two phase structures, namely matrix and microballoons. These foams are classified as closed pore foams due to the existence of porosity within the microballoons. However, during fabrication of syntactic foams, air or voids can be entrapped within the matrix. The presence of air or voids within the matrix is termed as open cell porosity and thus making syntactic foams a three phase structure. A schematic representation of two phase and three phase structures of syntactic foams are shown in Figure 2. The micro structure of syntactic foams under Scanning Electron Microscope (SEM) is shown in Figure 3. The SEM image showed the resin and microballoons phases at the cut surface of syntactic foam sample.

1.2.5 Motivation for Present Study

Published studies [16,19-21] have concluded that with the addition of nanoclay [22], and fiber [23] or by creating gradient structures, the mechanical performance of syntactic foams can be improved. As these materials are used in high performance applications, it is important to

increase the energy absorption of syntactic foams without losing the mechanical strength for achieving high fracture toughness. Studies [16] have shown that the energy absorption of syntactic foams can be increased dramatically with gradient structures. The gradient structure can be fabricated by two ways: either by changing the volume fraction of microballoons in each layer or by changing the radius ratio (η) of microballoon in each layer. The schematic representation of two gradient structures type syntactic foams are shown in Figure 4. Out of these two methods, the radius ratio (η) variant gradient syntactic foams have great design flexibility and control over final properties. Compressive properties are not found to be significantly improved in gradient structure fabricated with the variation in microballoon volume fraction [16]. Gupta et al. have created gradient structures with the variation in microballoon radius ratio (η) by using a foreign material such as adhesive between the layers. Even though compressive properties were found to significantly improve with Gupta et al. technique, adhesive layer in the interface is subjected to peeling stresses.

Therefore, in the present study, gradient structures are fabricated without using the adhesive material in between the layers. Furthermore, the study deals with the effect of layer sequencing on the compressive properties of gradient structures for the first time. Five different layer sequencing gradient structures are fabricated using four different microballoons, namely, S22, S32, S38 and K46. The four microballoons have a variation in radius ratio (η) and thus creating a variation in their densities. The volume fraction of microballoons in each layer of gradient structure is maintained constant at 60%. The overall density of five different layer sequencing gradient structures is maintained same. Fabricated gradient structures are tested for compression properties on MTS-810 servo hydraulic machine. In addition, impact analysis is performed on all gradient structures to study the effect of layer sequencing on dynamic

properties. Impact testing is performed using a Dynatup impact machine and the testing is performed at 1 m/s, 2 m/s and 3 m/s.

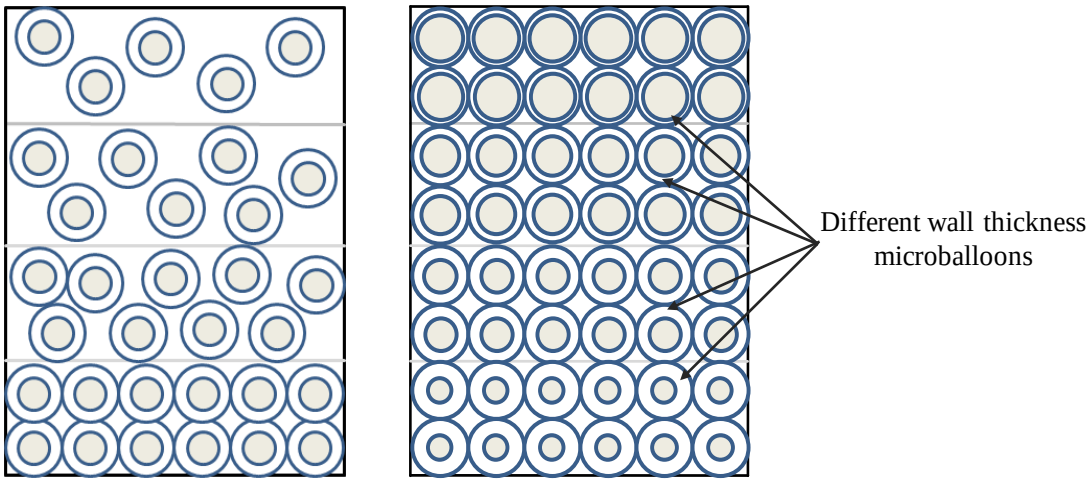

Figure 4 (a) Schematic representation of microballoon volume fraction variant Gradient structure (b). Microballoons radius ratio (η) variant Gradient structure

1.3 Thesis Organization

Chapter 1 gives a brief introduction to composites and its classification, syntactic foams (particulate composites) and its advantages and applications.

Chapter 2 includes the previous work performed to study various properties of syntactic foams. Synopsis of various studies performed to increase energy absorption, compressive strength by reinforcing syntactic foams with various fillers and fabricating gradient structures will be discussed.

Chapter 3 includes the description of various raw materials used in this study and fabrication procedure for fabricating gradient structures.

Chapter 4 includes the description about testing machines and standards used in this study.

Chapter 5 discusses the flat-wise and edge-wise compressive properties of gradient structures fabricating using technique developed in this study. Furthermore impact properties of gradient structures are discussed.

Chapter 6 presents conclusions and future work.

CHAPTER 2. LITERATURE REVIEW

Solid [24-25] and hollow [26-27] glass filled particulate composites are used as core materials in composite structures for various weight sensitive applications. Syntactic foams consisting of hollow glass particles (microballoons) in an epoxy matrix have gained significant importance as core materials in sandwich composites due to their high damage tolerance [18], low moisture absorption [28-29], and high specific compressive strength [30]. In order to fabricate syntactic foams with minimum air entrapment in the matrix, different fabrication techniques [18,31] were studied by researchers. It was found that the optimum resin-microballoon interface can be achieved with minimum void content.

Syntactic foams were used as buoyancy aid materials for under water applications due to their light weight and superior compressive properties [32-33]. Bunn et al. [32] fabricated syntactic foams using phenolic microballoons and studied the compressive properties with the variation in microballoons volume fraction. They found that the compressive strength of syntactic foams increased with a decrease in the microballoon volume fractions. Gupta et al. [33] fabricated syntactic foams using glass microballoons and studied the compressive properties with the variation in microballoons volume fraction. They found that the compressive strength of syntactic foams fabricated with glass microballoons was higher compared to syntactic foams fabricated with phenolic microballoons. Lin et al. [34] reported that the compressive strength of syntactic foams decreased with an increase in the glass microballoons volume fraction.

D'Almeida [8] studied the effect of the microballoon size on the compressive properties of syntactic foams. D'Almeida concluded that syntactic foams incorporated with smaller size microballoons show lower yield strength and modulus than syntactic foams incorporated with larger size microballoons. Gupta et al. [17-18] studied the effect of density variations of

microballoons on the compressive properties of syntactic foams. In order to understand the effect of radius ratio (η) and aspect ratio on the compressive properties of syntactic foams, Gupta et al. conducted compressive tests on syntactic foams fabricated using S22, S32, S37, S38, and K46 microballoons. The difference between five microballoons used in their study was the radius ratio (η) of microballoons and thus the density of microballoon in syntactic foam. Gupta et al. [17] observed that the compressive strength and modulus of syntactic foams were dependent on microballoon radius ratio (η) and specimen aspect ratio. Density of microballoon is dependent on the radius ratio (η). Higher value of radius ratio (η) leads to light weight and thin walled microballoon. On contrary, lower radius ratio leads to high density and thick walled microballoons [17,35]. Gupta et al. found that the compressive strength and modulus of syntactic foams incorporated with lower radius ratio (η) microballoons was higher compared to the syntactic foams with higher radius ratio (η) microballoons. They observed that the stress-strain curves of syntactic foams typically show a stress-plateau (Figure 5) similar to those of high energy absorption materials [35]. Lower density foams show a larger stress-plateau but lower strength compared to higher density foams. Larger stress plateau is a typical characteristic of high energy absorption materials. On contrary, higher density foams show high strength and lower plateau region.

Comparing flat-wise and edge-wise compression properties of syntactic foams fabricated with varying radius ratios (η), Gupta et al. [17] concluded that the edge-wise compressive modulus and compressive strength are superior to that of flat-wise compression properties. Gupta et al. observed that the edge-wise compression failure of foam specimens was due to vertical splitting caused by the shear cracks from corners. Kim et al. studied the compressive failure mechanism of syntactic foam having varying concentration of resin [36]. Kim et al.

concluded that longitudinal splitting and layer crushing of specimen takes place under compression.

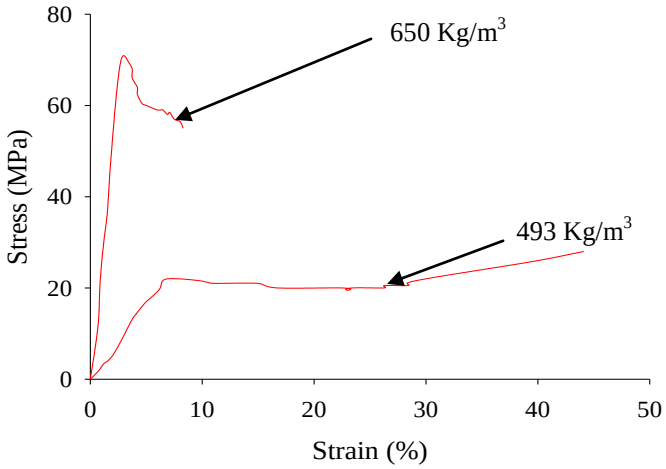

Figure 5 Stress plateau behavior with different density microballoons syntactic foams [35]

Effect of microballoon radius ratio (η) and volume fraction on the tensile properties of syntactic foams was studied by Gupta and Nagony [37]. They found that syntactic foams fabricated with high density microballoons exhibited high tensile strength and modulus. It was also found that the tensile strength and modulus values of syntactic foams decrease with an increase in volume fraction for similar density microballoons. Effect of microballoon volume fraction on the tensile behavior of syntactic foams was studied by Kishore et al. [38]. Kishore et al. concluded that the tensile modulus and strength increase linearly with a decrease in the microballoon volume fraction.

As syntactic foams are used in naval applications, understanding the effect of moisture on compressive properties of syntactic foams is important. Gupta and Woldesenbet performed hygrothermal studies [28] on syntactic foams to understand the effect of moisture on compressive properties. They concluded that the modulus value decrease with an increase in the

moisture content of the specimen. It was also observed that the compressive yield strength decrease with an increase in temperature.

In addition to quasi-static studies, dynamic studies of syntactic foams are also important due to their extensive use in sandwich structures for automobile applications [39-44]. It was found that the impact properties of syntactic foams increase with an increase in microballoon volume fraction [44]. Kim and Kamis [45] studied the effect of microballoons volume fraction on impact properties of syntactic foams. Kim and Kamis found that the impact energy absorption increase with an increase in the volume fraction of microballoons. Effect of microballoon wall thickness on dynamic response of syntactic foams was studied by Woldesenbet [46-47]. Woldesenbet concluded that syntactic foams fabricated with thinner wall microballoons possess lower initiation energy but higher propagation energy compared to syntactic foams fabricated with thicker wall microballoons. Also, the maximum load values sustained by syntactic foams in impact increased with an increase in the wall thickness of microballoons.

Due to the usage of these syntactic foams as core materials in sandwich structures, properties of sandwich structures need to be analyzed. Sandwich composites are fabricated by attaching two thin but stiff skins on both sides of the light weight core material. Gupta et al. [48] performed the compression tests on sandwich structures. Gupta et al. observed that the skin on the sandwich structure does not provide significant improvement in the flat wise compression properties compared to plain syntactic foams core. However, the edge wise compression properties are affected by the skin on the sandwich structure. The skin present on the sandwich structure increased the edge-wise compression properties compared to syntactic foam core. Rizzi et al. [49] performed compression and tensile tests on sandwich structures and concluded

that the tensile modulus of sandwich structures was higher than its compressive modulus. Li and Muthyala [50] studied the hybrid core sandwich structures as a combination of ortho-grid and foam core. They observed that the hybrid core sandwich structure provided a better elastic response and higher energy absorption. They have concluded that the better elastic response and higher energy absorption were due to the ability of syntactic foam core to absorb the energy of impact whereas, grid skeleton was able to stop the damage propagation due to impact. Li and Sandeep studied syntactic foams as a core material in iso-grid structures [51]. Compared to ortho-grid structures, the iso-grid structures resist different forces such as tension, compression, shear and flexural loads. With the same volume fraction of fiber and foam, iso-grid stiffened sandwich structures usually have higher initiation and propagation energy values when compared to the laminate structure.

Flexural properties of syntactic foam sandwich structures were studied by Gupta and Woldesenbet. They have performed three and four point bending and short beam shear test on syntactic foam core sandwich structures [52]. From their studies, Gupta and Woldesenbet concluded that the values of core shear stress and facing bending stress obtained in three-point and four-point tests were independent of wall thickness of microballoons. In short beam shear test, the core shear stress and facing bending stress were found to decrease with an increase in the wall thickness of microballoons. Flexural studies performed with microballoons volume fraction variation [24] concluded that the fracture toughness and flexural strength of syntactic foams sandwich structure decrease with an increase in the volume fraction of microballoons. Kim and Kemis [45] tested syntactic foam sandwich structures for flexural properties and concluded that the flexural modulus decreased with an increase in microballoon volume fraction.

High strain rate studies of syntactic foams are very important for design and analysis of composite structures under dynamic loading conditions [53-54]. The effect of wall thickness on high strain rate properties of syntactic foams were studied [55]. These studies observed that the peak strength and elastic modulus values of syntactic foams increased with an increase in the strain rate and/or wall thickness of microballoons. Composites fabricated with K46 microballoons (smaller radius ratio) showed higher strength, modulus and energy absorption as compared to composite foams having S22 microballoons at same strain rates [55]. Furthermore, compressive and high strain rate properties of syntactic foams fabricated with varying volume fraction and/or radius ratio (η) are widely studied in the published literature [56]. Studies concluded that the high strain properties decreased with an increase in the microballoon volume fraction and/or radius ratio (η). Yen et al. [57] found that the fracture resistance of syntactic foams increased with an increase in the strain rate.

In order to understand the distribution of porosity within the syntactic foam along with computation of mechanical properties, nondestructive characterization techniques such as ultrasonic, acoustic emission, eddy current can be performed. Ultrasonic studies of syntactic foams are very important in order to characterize the defects in the specimen during fabrication. The internal defects and structure of a material affect the quasi-static and dynamic properties. Also, ultrasonic studies are useful to observe the extent of damage occurred in syntactic foams during impact testing. Ray et al. [58] studied the air entrapment and defects in fiber reinforced particulate composites using non-destructive techniques such as thermal imaging, ultrasonic (A-scan and C-scan) and scanning electron microscopy. Mylavarapu and Woldesenbet [59] studied the effect of microballoon wall thickness and volume fraction on ultrasonic properties such as

velocity and attenuation. Through their studies, they were able to predict the dynamic modulus and Poison's ratio of syntactic foams using ultrasonic characterization.

With the usage of these syntactic foam materials in high performance applications, enhancement of energy absorption and mechanical properties of syntactic foams are required. Studies have shown that quasi-static and dynamic properties of syntactic foams can be improved by adding rubber particles, nanoclay, nanotubes, nanofibers, fibers. Gupta et al. studied the compressive properties of nanoclay reinforced syntactic foams and observed that the energy absorption increased by 80%-200% compared to plain syntactic foams [60]. Peter et al. [55] studied the compressive behavior of nanoclay syntactic foams and concluded that the compressive strength and modulus values were higher at 1% inclusion of nanoclay. Peter et al. also studied the effect of microballoon density on high strain rate compressive properties of syntactic foams. Peter et al. concluded that composite foams subjected to high strain rate showed higher strength and modulus as compared to those subjected to lower strain rates. Maharsia and Jerro [61] studied the tensile behavior of nanoclay included syntactic foams and concluded that the tensile strength increased with the inclusion of nanoclay. Woldesenbet studied the impact properties of nanoclay reinforced syntactic foams [46]. Woldesenbet concluded that the incorporation of nanoclay in syntactic foams increased the maximum load and initiation energy of both S22 and K46 microballoon syntactic foams. The peak strengths were achieved at 1% volume fraction of nanoclay addition in syntactic foam. Zheng et al. [62] found that the impact strength and modulus values of syntactic foams increased with an addition of nanoclay to matrix. Li and Nji [63] observed that the impact energy absorbed by the rubberized particle syntactic foam was higher compared to that of plain syntactic foams or pure epoxy.

Even though the energy absorption and strength of syntactic foams increased with nanoclay inclusion, agglomeration of nanoclay at volume fractions more than 1% is an obstacle for enhancement of material properties. Also, the mechanical properties of nanoclay reinforced syntactic foams were not found to be improved significantly due to agglomeration of nanoclay at higher microballoon volume fractions [55]. At higher microballoon volume fractions, stress concentrations and voids formed due to less amount of matrix and lack of uniform dispersion of nanoclay reduce the strength of the composites at all strain rates. In order to increase the energy absorption of syntactic foams without reducing the strength, researchers studied syntactic foams as gradient structures [16,64-66]. Gradient structures can be created either by varying the microballoons volume fraction or by varying the radius ratio (η) of microballoons. Initially the studies of Functionally Gradient Syntactic Foams (FGSFs) are synthesized with the variation in microballoons volume fraction (V_{mb}) along one dimension of the material structure. The FGSFs created with the variation in microballoons volume fraction showed a sudden drop of 40% - 60% in stress values immediately after attaining the peak compressive strength [16]. These studies have achieved limited enhancement in compressive properties compared to the plain syntactic foams. Gupta et al. [16] studied FGSFs with microballoons volume fraction variation and concluded that the energy absorption of microballoons volume fraction variant gradient structures is not found to be significantly improved. Additionally, these foams undergo non-uniform stress concentrations causing catastrophic failure originating in the matrix rich side of the specimen, especially when the matrix is a brittle polymer such as epoxy resin. Warping of the material after being exposed to changing temperature or moisture conditions due to the difference in the coefficient of thermal expansion also causes instability in the material.

In order to overcome some of these limitations, Gupta et al. [16,67] fabricated FGSF specimens with a gradient in the radius ratio (η) of microballoons. However, FGSF's were fabricated by joining syntactic foam layers using an adhesive bond. Gupta et al. observed that the energy absorption of FGSF's was more than that of plain foams. Also, no sudden drops in stress were observed after the peak strength. Gupta et al. also found that the properties of gradient structures always depend on the weakest layer of the configuration. However, it is evident that peeling stresses are high in adhesively bonded composites [68] and generally cause transverse failure. Also, the properties of adhesively bonded materials depend on the adhesive material in addition to matrix material, microballoon volume fraction and microballoon radius ratio (η). Due to this reason, FGSF specimens in the present study are fabricated without using any foreign material such as adhesive material in between the layers.

Even though several studies are performed to study the quasi-static and impact behavior of plain syntactic foams, very little information is available on quasi-static and dynamic analysis of gradient structures. Also, no study is available on the layer sequencing effect on compression and impact properties of gradient syntactic foams. As these materials are widely used in various high strength and high energy absorption applications, extensive study of quasi-static and dynamic properties of gradient syntactic foams is required.

Hence, in the current study a fabrication method is developed for gradient structures. Four types of microballoons namely S22, S32, S38, and K46 are used to create gradient structures based on variation in microballoons radius ratio (η). Five different layer sequencing configurations are fabricated to understand the layer sequencing effect on compression and impact properties of gradient structures. Out of these five configurations, four configurations are fabricated as symmetrical configurations and a fifth one as unsymmetrical configuration. Quasi-

static flat-wise and edge-wise compression tests are conducted on these gradient structures using Instron MTS-810 servo hydraulic machine. The compressive yield strength, energy absorption and modulus values are calculated in quasi-static test using load vs. elongation curve obtained during testing of these materials. The effect of layer sequencing on compressive properties along with advantages of this new fabrication technique over previous techniques are analyzed and discussed. Also, impact testing is performed on gradient structures with different layer sequencing on Instron Dynatup 8250 impact testing machine. The impact results of five gradient structures are compared to one another to understand the layer sequencing effect on impact properties.

CHAPTER 3. RAW MATERIALS AND FABRICATION

3.1 Raw Materials

3.1.1 Glass Microballoons

The glass microballoons used in this study are non-porous in nature and are manufactured and supplied by 3M Company under the trade name of 'Scotchlite'. Four types of microballoons, namely S22, S32, S38 and K46, are used in this study. These microballoons are hollow spherical particles of chemically-stable soda-lime-borosilicate glass. Physical properties of selected microballoons, supplied by the manufacturer, are presented in Table 1. Microballoon types S32, S38 and K46 selected for this research have the same mean outer diameter of 40 μm whereas microballoon type S22 has a mean outer diameter of 35 μm. The mean inner diameter is calculated by taking the difference in the average true particle density of solid and hollow particles made up of same material. Subsequently, the average wall thickness of microballoons is calculated. The difference in wall thickness of different types of microballoons causes the difference in their density. The calculated radius ratio (η) for all types of microballoons is also given in Table 1. The microballoon type in Table 1 is the manufacturer's code for the identification of selected microballoons.

Table 1 Microballoons size distribution and radius ratio

Micro Balloon Type	**Microballoon Size Distribution (μm)**			**Average True particle Density (kg/m^3)**	**Average Wall Thickness (μm)**	**Radius Ratio (η) 10th percentile**
	10th percentile	**50th percentile**	**90th percentile**			
S22	20	35	60	220	0.52	0.9703
S32	20	40	75	320	0.88	0.9561
S38	15	40	75	380	1,05	0.9474
K46	15	40	70	460	1.29	0.9356

3.1.2 Resin

Resin is a basic constituent in the matrix system. The epoxy resin diglycidylether of bisphenol-A (DGEBA) having a trade name D.E.R. 332 is used in this study. It is manufactured by DOW Chemical Company. D.E.R.332 has a tendency to crystallize if stored at a temperature below 25°C [69]. Crystallization is induced by the chilling and seeding of dust particles or incorporation of filler materials. On the other hand, D.E.R 332 can regain its liquid state by heating at 50-55°C, and the heating process of resin does not affect its performance [70]. However, long-term warm storage may result in slight discoloration. The typical properties of D.E.R 332 given by DOW Chemical Company are mentioned in Table 2.

Table 2 D.E.R 332 epoxy resin typical properties

Properties	**Values**
Density at 25 °C	1160 kg/m^3
Flash point	252 °C
Viscosity at 25 °C	4000-6000 mPas
Appearance	Clear liquid
Weight at 25 °C	9.7 lbs/Gal
Shelf life	24 months

3.1.3 Diluent

C_{12}-C_{14} aliphatic mono-glycidyl ether is used in the matrix system as a diluent to reduce the viscosity of resin. It has a trade name of Erisys GE-8 and is manufactured and supplied by CVC Specialty Chemicals. The compatibility of diluent with epoxy resin at all concentrations is studied [71]. The amount of diluent used in the resin system, affects the gel time and curing

properties [71]. In this study, diluent is used at 5% volume fraction of matrix system. The typical properties given by CVC chemicals are mentioned in Table 3.

Table 3 Typical properties of Erisys GE-8 diluent

Properties	**Values**
Density	890 kg/m^3
Flash point	95 °C
Viscosity at 25 °C	5-10 mPas
Appearance	Clear liquid, clean
Weight at 25 °C	7.4 lbs/Gal

3.1.4 Hardener

Hardener D.E.H 24 is used as a curing agent for the fabricated sample. D.E.H 24 is a liquid aliphatic polyamine curing agent called triethylene-tetra-amine (TETA). Due to its hygroscopic nature [72], D.E.H.24 is stored in its original closed packaging. In this study, hardener is used at 13% volume fraction of matrix system. The typical properties of hardener given by DOW chemicals are mentioned in Table 4.

Table 4 Typical properties of D.E.H 24 epoxy curing agent

Properties	**Values**
Density	981 kg/m^3
Flash point	118 °C
Viscosity at 25 °C	27 mPas
Appearance	Clear liquid
Shelf life	24 months

3.2 Fabrication Method

Five different configurations of IFGSF composites as shown in Figure 6 are fabricated in this study. Four types of microballoons, namely, S22, S32, S38, and K46 are used in this study to fabricate the gradient structures. Symmetric and unsymmetrical configurations of gradient structures are fabricated. In symmetric IFGSF composites, two of the four microballoons are used. One unsymmetrical configuration of IFGSF structure is fabricated using all four microballoon types. The unsymmetrical IFGSF configuration is fabricated to show the advantages of this layer over layer integrated technique over adhesively bonded technique used in Gupta et al. [16]. For comparing the IFGSF structure with adhesively bonded FGSF, IFGSF structure is fabricated with the same layer sequencing to that of adhesively bonded FGSF structure. The volume fraction of microballoons is maintained constant at 60% in each of the syntactic foam layer. The overall density of all IFGSF samples is maintained constant. For fabrication of IFGSF structure, the resin is preheated in an oven at 50-55 °C for 24 hours to restore to its liquid state. This reduces the viscosity of resin and helps in better wetting of microballoons during mixing. The resin is then removed from the oven and 5% diluent is added to further reduce its viscosity. The mixture is cooled to ambient temperature before hardener is added as a rise in temperature of mixture could lead to exothermic reaction damaging the composite. Hardener is added after the resin mixture is cooled to ambient temperature. This final mixture is called matrix system. To this resin mixture, microballoons are mechanically mixed carefully without breaking. The microballoon and resin mixture is poured in the square aluminum mold as shown in Figure 7. The thickness of each syntactic foam layer is maintained by using aluminum strips on each side of the mold. The inner volume of the mold cavity is $305\times305\times20$ mm^3. Flatness of the each layer is maintained using a level indicator. Before the

second layer is poured over the base layer, the base layer is allowed to partially solidify. Additional layers are prepared in the second mold as mentioned above and laid over the base layers to prepare IFGSF structure. This process continues until all the layers are set.

The fabricated IFGSF structure is kept under vacuum for 30 to 45 min to reduce the void content. Figure 8 – Figure 14 show the pictorial representation of layer over layer integrated fabrication technique for gradient structures. Casted IFGSF slabs are cured at room temperature for 24 hours and post cured at 100±3°C for 3 hours. Figure 15 shows the fabricated IFGSF composite foam after post curing process is completed. In order to show the enhancement of compression properties of IFGSF structures, plain syntactic foams with similar density are fabricated using the same method as that of individual layers of IFGSF composite.

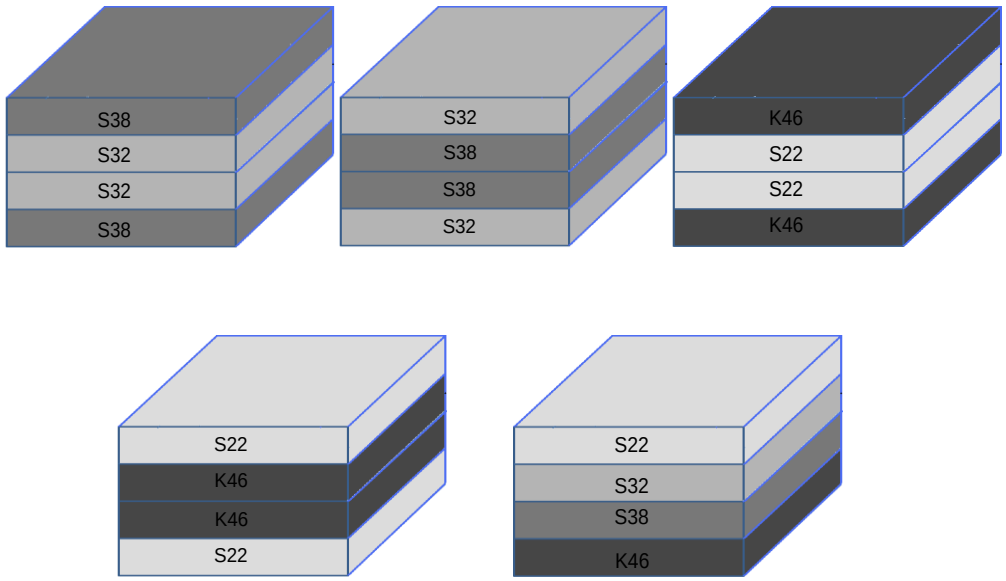

Figure 6 Pictorial representation of five IFGSF configurations

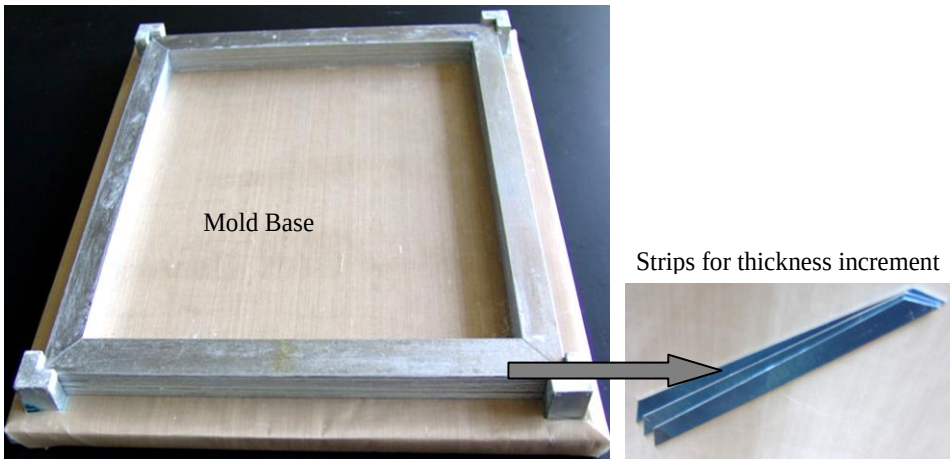

Figure 7 Schematic representation of mold assembly and strips

Figure 8 Syntactic Foam Mixture is poured in Base Mold

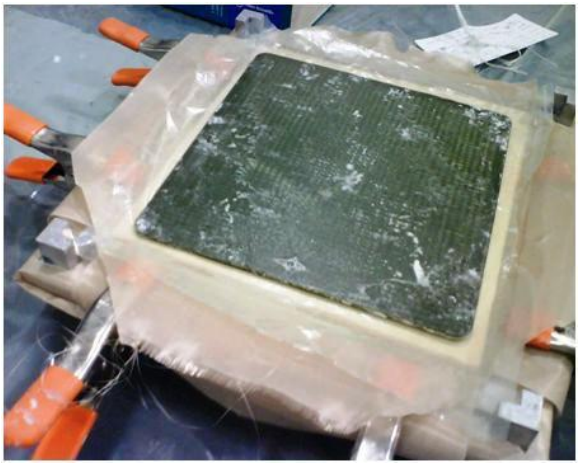

Figure 9 Leveling the base layer to achieve the perfect flat surface

Figure 10 Glass plate covered with Teflon kept over second mold for second layer fabrication

Figure 11 Prepared second layer over glass plate is integrating with the base layer

Figure 12 Perfect arrangement of second layer to align with the base layer

Figure 13 Uniform force is applied over integrated layers of gradient structure

Figure 14 Remove the glass plate from gradient structure after perfect layer integration

Figure 15 Final fabricated IFGSF sample

3.3 Density Measurement

The density of the fabricated syntactic foam composites is measured using ASTM C 271-94 standard [73]. Porosity is one factor, which affects the properties of syntactic foams. The fabricated samples have porosity within the microballoons, known as closed cell porosity and also in the matrix material due to mechanical mixing process, known as open cell porosity. Calculated values of density and open cell porosity (void content) of fabricated syntactic foams are shown in Table 5.

Table 5 Measured densities and open cell porosity in FGSF configurations

FGSF Configuration	**Theoretical Density (kg/m^3)**	**Density(kg/m^3)**		**Open Cell Porosity (%)**	
		Flat-wise Sample	**Edge-wise Sample**	**Flat-wise Sample**	**Edge-wise Sample**
K46-S38-S32-S22	655	629 ± 4.8	640.2±2.3	3.96 ± 0.7	2.38±0.2
K46-S22-S22-K46	652	623 ± 4.6	638.6±2.8	4.50 ± 0.7	2.28±0.3
S22-K46-K46-S22	658	627 ± 4.2	641.5±3.0	3.83 ± 0.6	2.10±0.2
S32-S38-S38-S32	658	622 ± 2.4	635.7±1.5	5.45 ± 0.4	3.40±0.2
S38-S32-S32-S38	658	628 ± 4.9	638.6±3.5	4.55 ± 0.7	3.34±0.2

CHAPTER 4. EXPERIMENTAL SETUP

4.1 MTS-810 Servo Hydraulic Machine

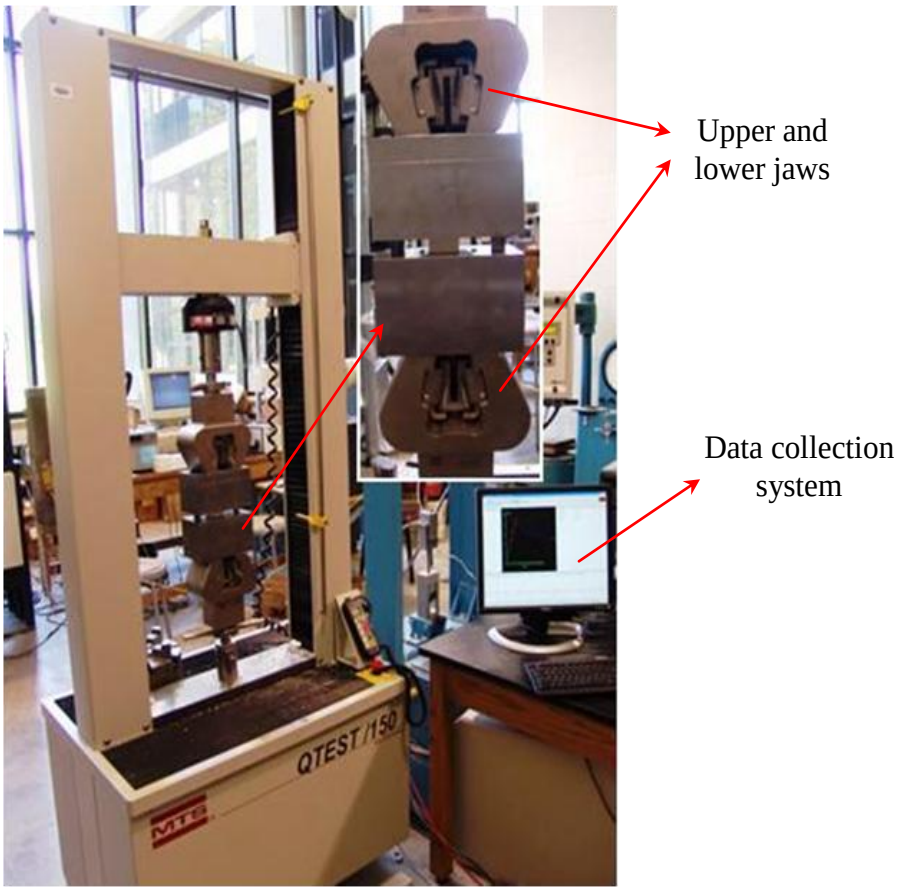

Figure 16 Instron MTS-810 servo hydraulic machine

In this research work, quasi-static flat-wise and edge-wise compression tests are conducted on IFGSF structures using Instron MTS-810 servo hydraulic testing machine as shown in Figure 16. An Instron Data Acquisition software is used to acquire data from the machine during testing. In the present study, the crosshead speed is maintained at 1.3 mm/min. Five specimens from each IFGSF configuration are tested to show the repeatability of results. Load and displacement values are acquired from the MTS machine.

4.2 Instron-8250 DYNATUP Impact Testing Machine

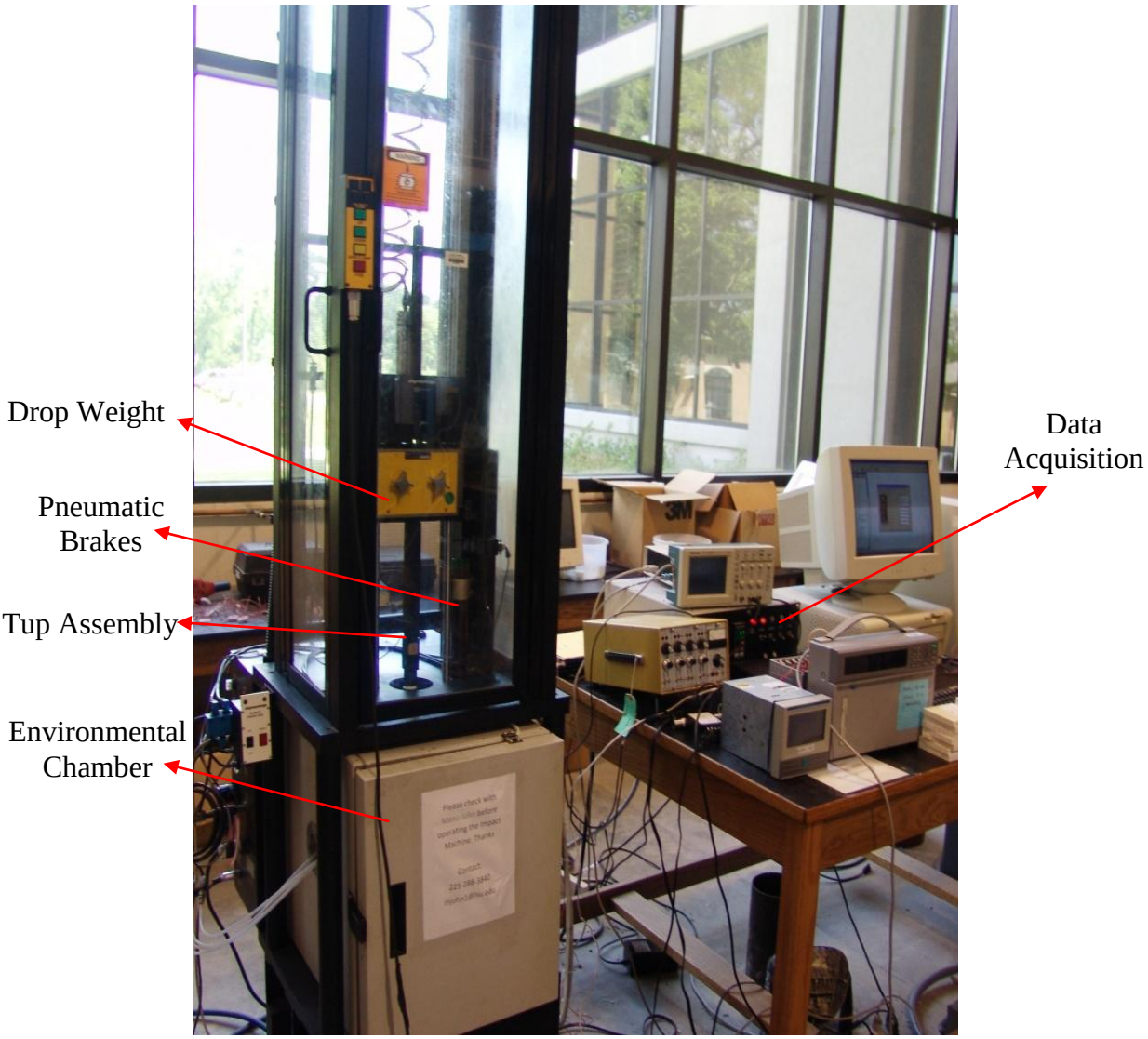

Figure 17 Instron Dynatup 8250 impact testing machine

In this study, Instron Dynatup 8250 machine is used for impact testing of IFGSF structures as shown in Figure 17. The tup assembly of impact machine is shown in Figure18. During testing, the impact data is acquired by using Impulse Data Acquisition software. Load, energy, displacement and velocity readings with respect to time are acquired by the software. Data is plotted and the initiation, propagation and maximum energies, along with maximum load

sustained by the specimen are calculated. The energy corresponding to the maximum load in the load vs. time curve is called initiation energy. Initiation energy is defined as the amount of strain energy transferred elastically by the target [63]. Initiation energy can be also defined as the energy absorbed by the material before initiation of failure. Propagation energy is defined as the difference between maximum impact energy and the initiation energy [63]. Propagation energy is nothing but the energy absorbed by the specimen during failure. For example, the energy required to crush or fracture microballoons is accounted as propagation energy in this study. The energy absorbed by the specimen for progression of micro cracks into macro cracks is also accounted in propagation energy [63]. In this study, impact testing is performed on IFGSFs at three different impact velocities of 1m/s, 2m/s and 3m/s with a hammer weight of 3.4kg.

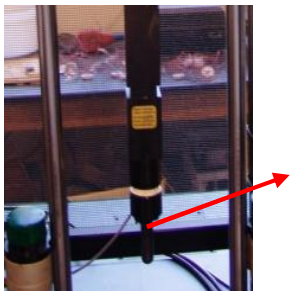

Figure 18 Dynatup impact machine tup assembly

4.3 Quasi- Static Flat-Wise Compression Standard and Specimen Size

Five samples of each of the five IFGSF configurations are tested for quasi static flat-wise compression properties using servo-hydraulic MTS machine according to ASTM C 365/C 365M-05 standard [74]. The sample dimensions in quasi-static compression tests are maintained at approximately 32×32×16 mm^3. Samples are compressed at a loading rate of 1.3 mm/min. Load, displacement and compressive yield strength values are recorded for each of the samples in compression testing.

4.4 Quasi- Static Edge-Wise Compression Standard and Specimen Size

Five samples of each of the five IFGSF configurations are tested for quasi static edge-wise compression properties using servo-hydraulic MTS machine according to ASTM D 695-96 standard [75]. The sample dimensions in quasi-static compression tests are maintained at 16×16×32 mm^3. Samples are compressed at a loading rate of 1.3 mm/min. Load, displacement and compressive yield strength values are recorded for each of the samples in compression testing.

4.5 Impact Testing Standard and Specimen Size

Three samples from each type of IFGSF configuration are tested for impact properties on DYNATUP model 8250 impact machine. Sample dimensions are maintained at 101.6 x 101.6 x 16 mm^3 (equivalent to 4 x 4 x 0.6 $inch^3$). The mass of the drop-weight and tup assembly used in impact testing is 3.4 kg. The impactor has a hemispherical tup of 16 mm diameter. The impact velocities used are 1, 2 and 3 m/s with an error of $\pm$0.16 m/s in the machine.

4.6 Ultrasonic Inspection

Ultrasonic testing is performed on the fabricated IFGSF structure to know the internal voids and disbands at layer interface. The ultrasonic testing apparatus used in this research is UltraPac, manufactured by the Physical Acoustics Laboratory (Princeton, NJ, USA). It is a water immersion system that can be used in pulse-echo and through-transmission test modes (Figure 19). The machine is run by ULTRAWIN software equipped with a programmable pulse receiver board (PAC-IPR-100) with 100 MHz bandwidth and a digitizer card (PAC-AD-500) with 500 MHz base sampling rate. The system is automated with three electric motors for the different axes motions and an electric motor control.

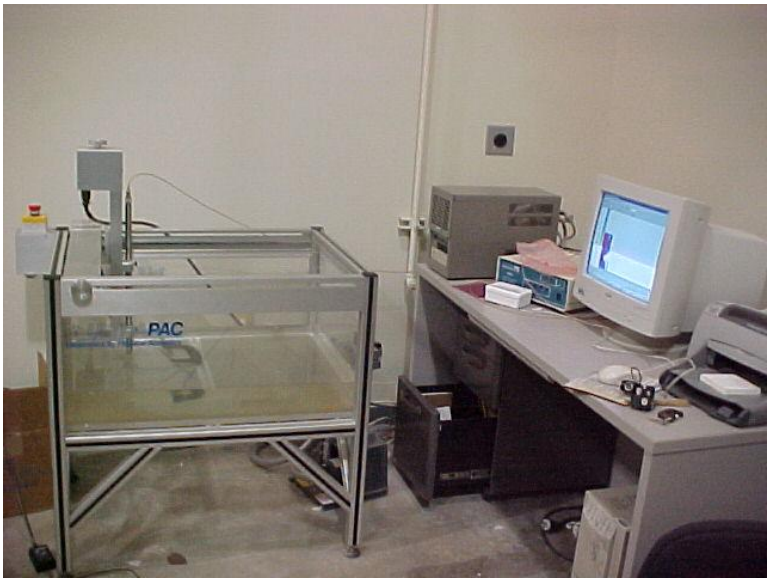

Figure 19 Ultrasonic testing machine used to perform C-scan

CHAPTER 5. RESULTS AND DISCUSSIONS

Compression properties and low velocity impact properties of IFGSF structures with different layer sequencing are analyzed in this study. Out of the five configurations, four IFGSF configurations namely, S22-K46-K46-S22, K46-S22-S22-K46, S32-S38-S38-S32, and S38-S32-S32-S38 have symmetric configurations, while K46-S38-S32-S22 is an unsymmetrical configuration. In order to show the advantage of IFGSF fabrication technique over adhesively bonded FGSF technique, unsymmetrical configuration is fabricated using the similar layer sequencing to that of adhesively bonded FGSF layer sequencing. The IFGSFs are tested for flat-wise and edge-wise compression properties. Flat-wise compression properties are compared with compression properties of plain syntactic foams and with adhesively bonded FGSFs. Edge-wise compression properties of IFGSFs are compared with edge-wise compression properties of plain syntactic foams with similar density. In order to study the effect of layer sequencing on compression properties of IFGSFs, the results from different configurations are compared to one another. Furthermore, the crack propagation behavior of flat-wise and edge-wise IFGSFs are monitored and analyzed with SEM and OM.

In addition to quasi-static compression properties, low velocity impact analysis is performed on five different layer sequencing IFGSF specimens using Instron Dynatup 8250 impact machine. The maximum load, initiation energy and propagation energy values are recorded from load vs. time and energy vs. time plots.

5.1 Flat-Wise Compression

The stress-strain graphs obtained from flat-wise compression testing of IFGSF are shown in Figure 20. Repeatability observed in five different specimens of each type of IFGSF configuration is also shown in Figure 20. It is observed that the scattering in the stress-strain

graphs is very small. Flat-wise compressive modulus, yield strength and energy absorption values are calculated from stress-strain graphs and are shown in Table 6. Flat-wise compressive modulus for different IFGSF configurations is calculated using ASTM standard C 365/C 365M-005 [74]. Energy absorption values of IFGSFs are calculated by calculating the area under the stress-strain plot.

A comparison of stress-strain graphs of IFGSF and plain syntactic foams is shown in Figure 21. From Figure 21, it can be observed that the stress-strain plateau of IFGSF extends from 8% to 60% strain in contrast to an extension from 10% to 20% for plain syntactic foams with similar density. Therefore, compared to plain syntactic foams, the energy absorptions of K46-S22-S22-K46, S22-K46-K46-S22, S38-S32-S32-S38, S32-S38-S38-S32 and K46-S38-S32-S22 IFGSFs are increased by 210%, 263%, 230%, 280% and 240%, respectively. This increase in energy absorption can be attributed to the high energy absorption by low density layers. The low density layers take high energy due to their high densification of microballoons. The high density layers in IFGSF contribute more to the strength of the IFGSF structure.

Table 6 Flat-wise compressive properties of plain and IFGSF configurations

Type of FGSF Specimen	**Average Compressive Modulus (MPa)**	**Average Compressive Yield Strength (MPa)**	**Energy Absorption (MPa-mm/mm)**
S22-K46-K46-S22	703.3±10	42.54±0.9	31.0±1.2
K46-S22-S22-K46	722.7±20	42.72±1.6	26.42±0.5
S32-S38-S38-S32	795.0±15	60.34±0.3	32.50±0.2
S38-S32-S32-S38	783.9±13	60.89±0.8	28.22±0.6
K46-S38-S32-S22	722.4±17	49.38±1.4	28.98±0.5
Plain Foam	585.7±6	47.90±1.7	8.54±0.4

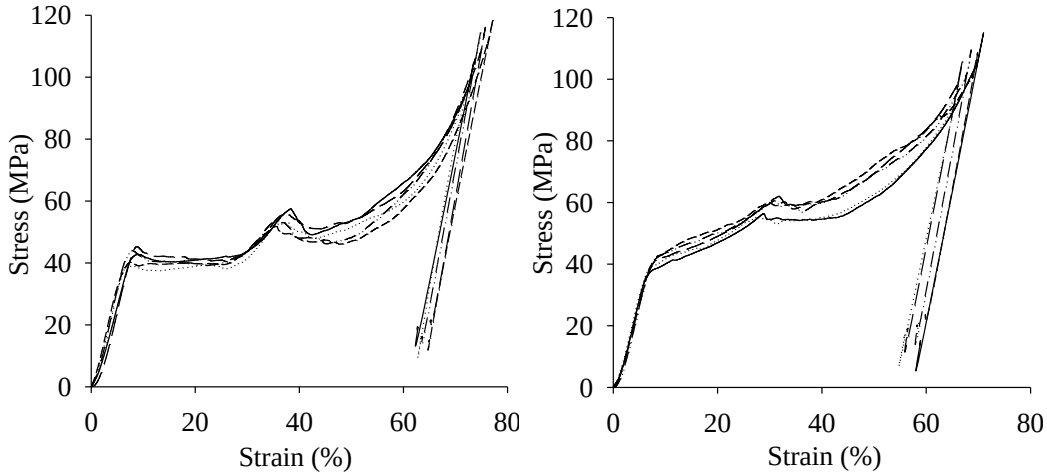

(a) K46-S22-S22-K46 IFGSF structure (b) S22-K46-K46-S22 IFGSF structure

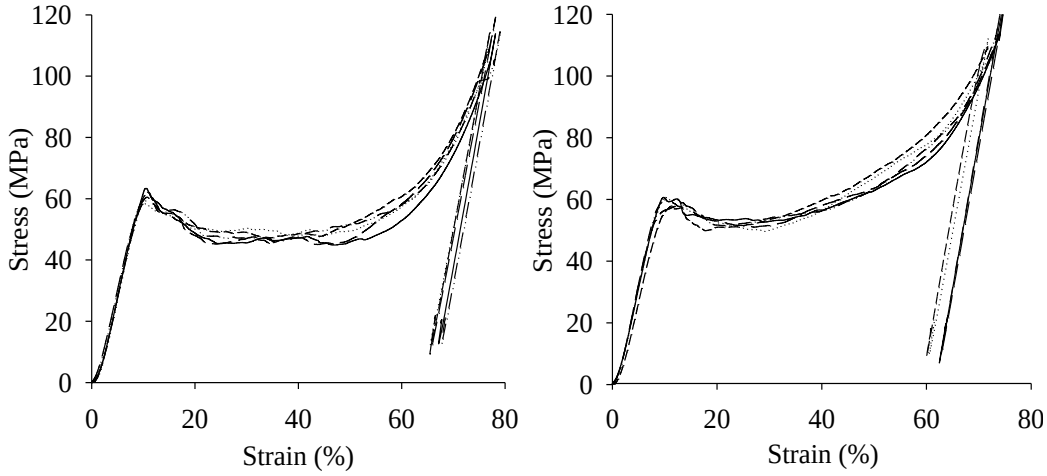

(c) S38-S32-S32-S38 IFGSF structure (d) S32-S38-S38-S32- IFGSF structure

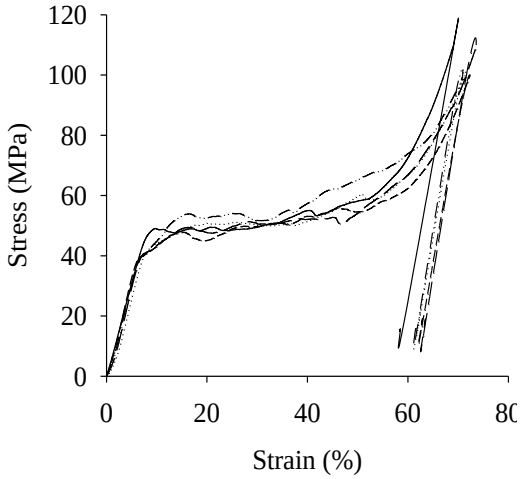

(e) K46-S38-S32-S22 IFGSF structure

Figure 20 Stress-Strain plots of IFGSF configurations to show the repeatability

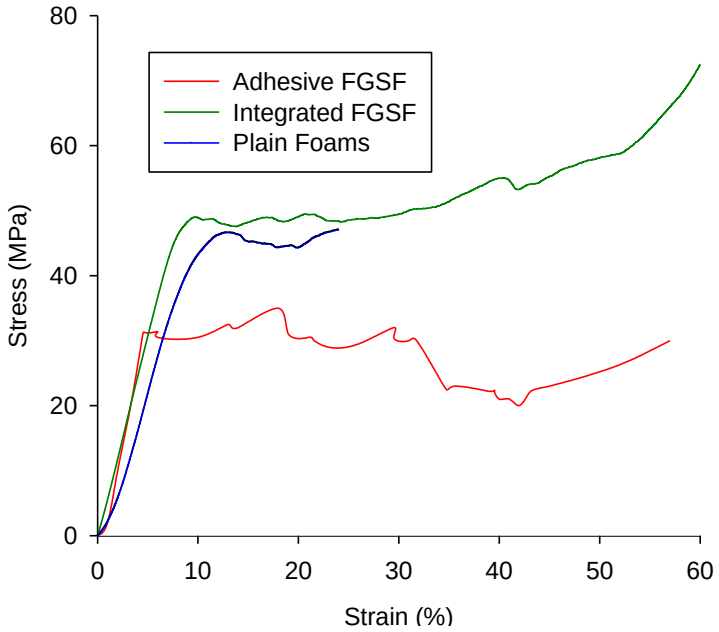

Figure 21 Stress- strain plots comparison of IFGSF,adhesive FGSF and plain foam

Comparing to adhesively bonded FGSF, it is also observed that there is an improvement in compressive yield strength and energy absorption values of IFGSFs (Figure 21). It is evident that the compressive yield strength values have increased from around 32.7 MPa for adhesively bonded FGSF to 49 MPa for IFGSF, an increase of 50%. Additionally, it is found that the overall energy absorption of IFGSF (28.9 MPa-mm/mm) is found to be 75% more than the energy absorption of adhesively bonded FGSFs (16.5 MPa-mm/mm). The increase in compressive properties of IFGSFs can be attributed to the difference in interfacial bonding between the two fabrication methods. In this study, gradient structures are fabricated by layer over layer integrated technique using the chemical interaction between layers rather than a foreign material such as an adhesive material. The compressive properties of adhesively bonded FGSF specimens are also dependent on the adhesive material in addition to the matrix material, type of microballoon, volume fraction of microballoons, and radius ratio (η). In addition, peeling stresses are present in adhesively bonded FGSF structures. However, peeling stresses

are found to be minimal in IFGSFs. Therefore, it can be concluded that the layer over layer integrated technique enhances the compressive properties of gradient structures as compared to adhesively bonded FGSF technique.

In order to study the effect of layer sequencing on the compression properties of gradient structures, stress-strain graphs from different IFGSF configurations are compared to one another and are shown in Figure 22. From Figure 22 and Table 6, it is found that the compressive yield strength, modulus and energy absorption values of S32-S38-S38-S32 and S38-S32-S32-S38 IFGSFs are higher compared to S22-K46-K46-S22, K46-S22-S22-K46 and K46-S38-S32-S22 IFGSF configurations. This difference in compressive properties between IFGSFs is due to the weakest layer effect on the flat-wise compressive properties of IFGSF configurations. The weakest layer in S32-S38-S38-S32 and S38-S32-S32-S38 configurations is S32, whereas in S22-K46-K46-S22, K46-S22-S22-K46 and K46-S38-S32-S22 configurations are S22. The S22 microballoon has higher radius ratio, lower density, and lower strength compared to S32 microballoon. Therefore the S32-S38-S38-S32 and S38-S32-S32-S38 IFGSFs have superior compressive properties compared to other IFGSFs used in this study.

From Figure 22, it is also found that all stress-strain plots of symmetric IFGSF configurations do not follow a similar trend. It is observed that the stress-strain curves obtained from S32-S38-S38-S32 and S38-S32-S32-S38 increased until yield point and then continued a flat trend until 50% of strain. Further, the curve slope increased dramatically after 60 % of strain and reached a consolidation point. However, the stress-strain curves of S22-K46-K46-S22 and K46-S22-S22-K46 IFGSFs did not follow a smooth stress-strain curve. In these configurations, the curves tend to peak at 30% strain corresponding to the stress level where the cracks propagate into the K46 layer due to the influence of secondary tensile stresses. Due to the

propagation of crack through K46, a fall in stress value is observed (Figure 22). Further, the curves followed a smooth increasing trend until 60% of strain, ultimately reaching to its consolidation point. The difference in stress-strain plots is due to the difference in the radius ratio (η) of the microballoons in those IFGSF configurations. The radius ratio difference (η) between S32 and S38 microballoons is small compared to the radius ratio difference between K46 and S22 microballoons. In S22-K46-K46-S22 and K46-S22-S22-K46 IFGSF configurations, the densification of S22 completes at 25 to 30% of strain. Thereafter K46 microballoons resist deformation until the individual K46 syntactic foam layer attains its yield stress limit. On contrary, in S32-S38-S38-S32 and S38-S32-S32-S38 IFGSFs, as the radius ratio (η) difference between S32 and S38 microballoons is small, the densification and crack propagation of S32 and S38 layers happens simultaneously. This is caused by smaller yield strength differences between S32 and S38 syntactic foams compared to the yield strength differences between K46 and S22 syntactic foams.

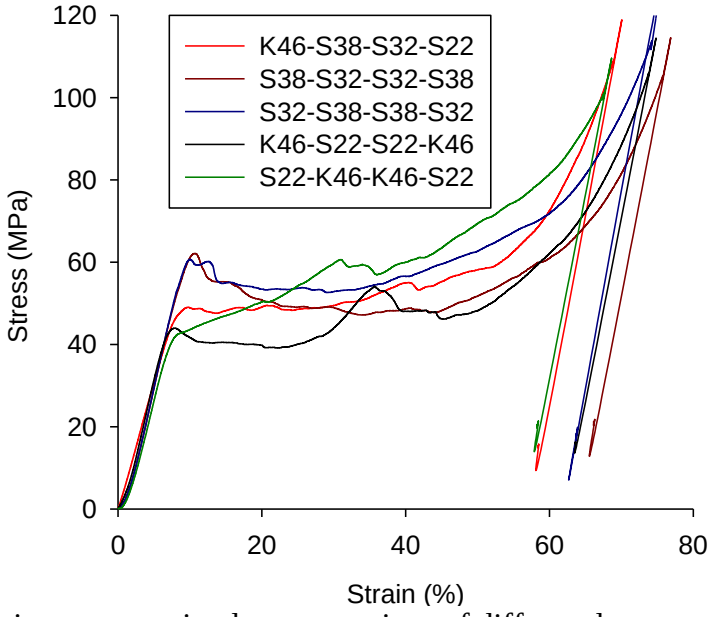

Figure 22 Flat-wise stress strain plots comparison of different layer sequencing IFGSFs

From Figure 22 and Table 6, it is also found that the energy absorption values in IFGSFs with central denser layers such as S22-K46-K46-S22 and S32-S38-S38-S32 are higher compared to their counter configurations. Additionally, the IFGSFs with central denser layers arrangements are structurally more stable. It is evident that the failure of structures always initiate at the weakest point. Therefore, the integrated structures with two weakest layers (low density layers) at the center have more localized failures. On further loading the micro localized failures become macro failures within short period time thereby causing overall structural instability. However, the IFGSFs with two stiffer layers at the center are structurally stable due to the smaller number of localized failures. Also, the stiffer layers at the center resist deformation until the development of higher stresses because of their locations sandwiched between the weaker layers. Thus, it is evident that compression properties of IFGSFs are affected by the layer sequencing.

The layer sequencing effect on the crack propagation behavior of IFGSF structures is monitored and the crack propagation images of different configurations used in this study are shown in Figure 23. In all IFGSF configurations, densification of microballoons and initiation of crack always takes place in the weakest layer (lower density layer) and then propagates towards the higher density layers upon loading, as shown in Figure 23. In flat-wise compression, even though equal compressive stress is applied on all the layers of IFGSF structure, because of the low density layers having low strength compared to high density layers, the crack initiates in the low density layer. From Figure 23(a), it is found that in K46-S38-S32-S22 IFGSF configuration, the crack is initiated in the weakest layer, S22, and then propagates through S32, S38, and K46 layers upon further loading. From Figure 23(b) and Figure 23(c), it is observed that in S32-S38-S32-S38 and S38-S32-S32-S38 IFGSF configurations, the crack is initiated in the weakest layer

S32, and then propagates to S38 layer as the load increased. Even in S22-K46-K46-S22 and K46-S22-S22-K46 IFGSF configurations, the crack is initiated in the weakest layer S22 and propagates towards the higher density layer K46 as the load increased.

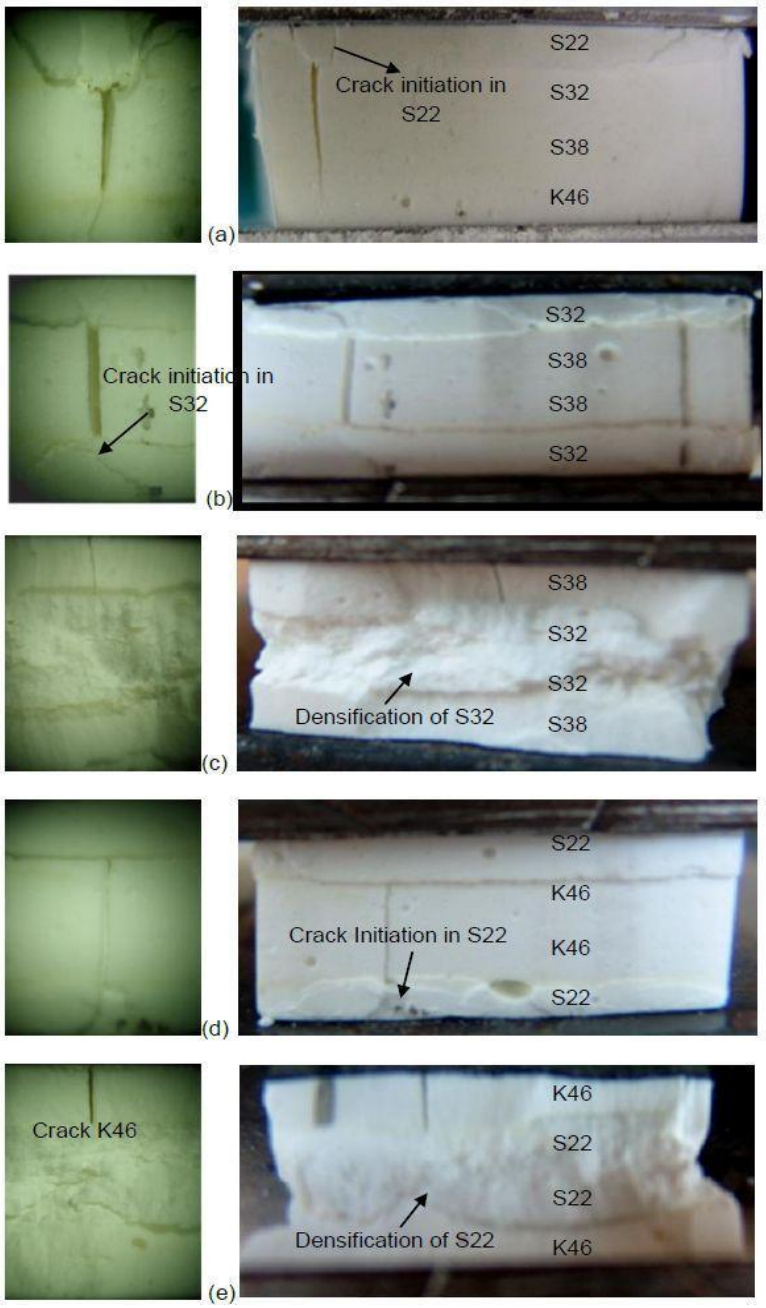

Figure 23 (a) Crack initiation and densification of S22 layer. (b) Crack initiation and densification of S32 layer. (c) Densification of S32 and crack through S38 layer. (d) Crack initiation and densification of S22. (e) Densification of S22 and crack through K46

However, the crack propagation behavior is found to be varying with the layer sequencing of the IFGSF configuration. From Figure 23(b) and Figure 23(c), the crack propagation behavior of S32-S38-S38-S32 and S38-S32-S32-S38 IFGSFs are different even though they are fabricated with S32 and S38 microballoons. In the configuration with S38 layers in the central plane (S32-S38-S38-S32) (Figure 23(b)), the crack propagates through the two denser layers (S38) of the IFGSF with partial densification of the S32 layers. The denser layers (stiffer layers) together at the center sustain more compressive stress compared to the same placed as outer single layers in the IFGSF structure. However, from Figure 23(c), it can be observed that in S38-S32-S32-S38 configuration, the complete densification and crushing of S32 layers is preceded by the crack propagation into the S38 layers. This is due to the weaker layers together at the center have more localized failures compared to stiffer layers together at the center. These micro localized failures in weaker layers become macro failures causing structural instability and peeling at the edges of the weaker layer S32. Also, weaker layers together allow more deformation without creating any failure in stiffer layers until their complete densification.

Also, the difference in crack propagation behavior of S32-S38-S38-S32 and S38-S32-S32-S38 IFGSFs is attributed to the fact that S32 layer in the central plane (S38-S32-S32-S38) has partial structural instability due to more localized failures of microballoons in the central layer. This structural instability is characterized by sliding and shear of S32 layer as well as peel out of part of S32 layer edges caused by secondary tensile stresses. The energy absorption in the S32-S38-S38-S32 IFGSF configuration is also found to be more compared to that of S38-S32-S32-S38 layer due to the same reason.

From Figure 23(d) and Figure 23(e), the crack propagation behavior of S22-K46-K46-S22 and K46-S22-S22-K46 IFGSFs are different even though they are fabricated with S22 and

K46 microballoons. In the configuration with K46 layers in the central plane (S22-K46-K46-S22), the crack propagates through the two denser layers (K46) of the IFGSF with partial densification of the S22 layers (Figure 23(d)). The denser layers (stiffer layers) together at the center sustain more compressive stress compared to the same placed as outer single layers in the IFGSF structure. However, from Figure 23(e), it can be observed that the complete densification and crushing of S22 layers is preceded by the crack propagation into the K46 layers. This is due to the weaker layers together at the center have more localized failures compared to stiffer layers together at the center. These micro localized failures in weaker layers become macro failures, which cause structural instability and peeling at the edges of the weaker layer S22. Also, weaker layers together allow more deformation without creating any failure in stiffer layers until their complete densification.

Also, the difference in crack propagation behavior of S22-K46-K46-S22 and K46-S22-S22-K46 IFGSFs is attributed to the fact that S22 layer in the central plane (K46-S22-S22-K46) has partial structural instability due to more localized failures of microballoons in the central layer. This structural instability is characterized by sliding and shear of S22 layer as well as peel out of part of S22 layer edges caused by secondary tensile stresses. The energy absorption in the S22-K46-K46-S22 IFGSF configuration is also found to be more compared to that of K46-S22-S22-K46 layer for the same reason.

From Figure 24, it is found that the densification of each layer initiates after attaining the yield strength of that particular microballoon layer. However, few microballoons break before this condition due to the localized failures of microballoons. The crack is found to propagate from lower density layers, S22 and S32, to higher density layers, K46 and S38, without any densification in S38 and K46 layers due to their brittle and stiffer nature.

Figure 24(a) – Figure 24(d) show the crack propagation behavior of unsymmetrical configuration under SEM. Figure 24(a) shows the densification of S22 and S32 microballoons at layer interface in unsymmetrical configuration. Figure 24(b) - Figure 24(d) show the SEM images inside the crack in S32, S38, and K46 layers of unsymmetrical configuration. From Figure 24(b), it is evident that the S32 microballoons inside the crack are partially broken. Whereas, the S38 and K46 microballoons inside the crack are not broken even though the crack propagated through those layers due to their brittle nature and high strength. Also, it is found that the crack propagation from weaker layers through stiffer layers is due to the matrix failure and interfacial bonding failure between matrix and stiffer microballoons. The densification differences are due to the difference in yield strength values of individual microballoon layers caused by the radius ratio (η) of microballoons in IFGSF structure. Higher strength is a typical characteristic of higher radius ratio (η) microballoon.

Figure 24(e) and Figure 24(f) are the SEM images of the K46-S22-S22-K46 IFGSF configuration. Figure 24(e) shows the densification of S22 microballoons and unbroken K46 microballoons at layer interface in K46-S22-S22-K46 IFGSF configuration. The K46 microballoons layer is stiffer and stronger due to their high radius ratio (η) compared to S22 microballoons layer. Furthermore, Figure 24(f) shows the microballoons inside the crack of K46 layer in the same IFGSF configuration. The crack is propagated through K46 layer before any densification starts. This is due to the matrix failure and interfacial bonding failure between matrix and K46 microballoon. Also, the K46 layer is brittle and stiffer compared to S22 layer. Similar densification and crack propagation behavior is observed in all IFGSF configurations used in this study.

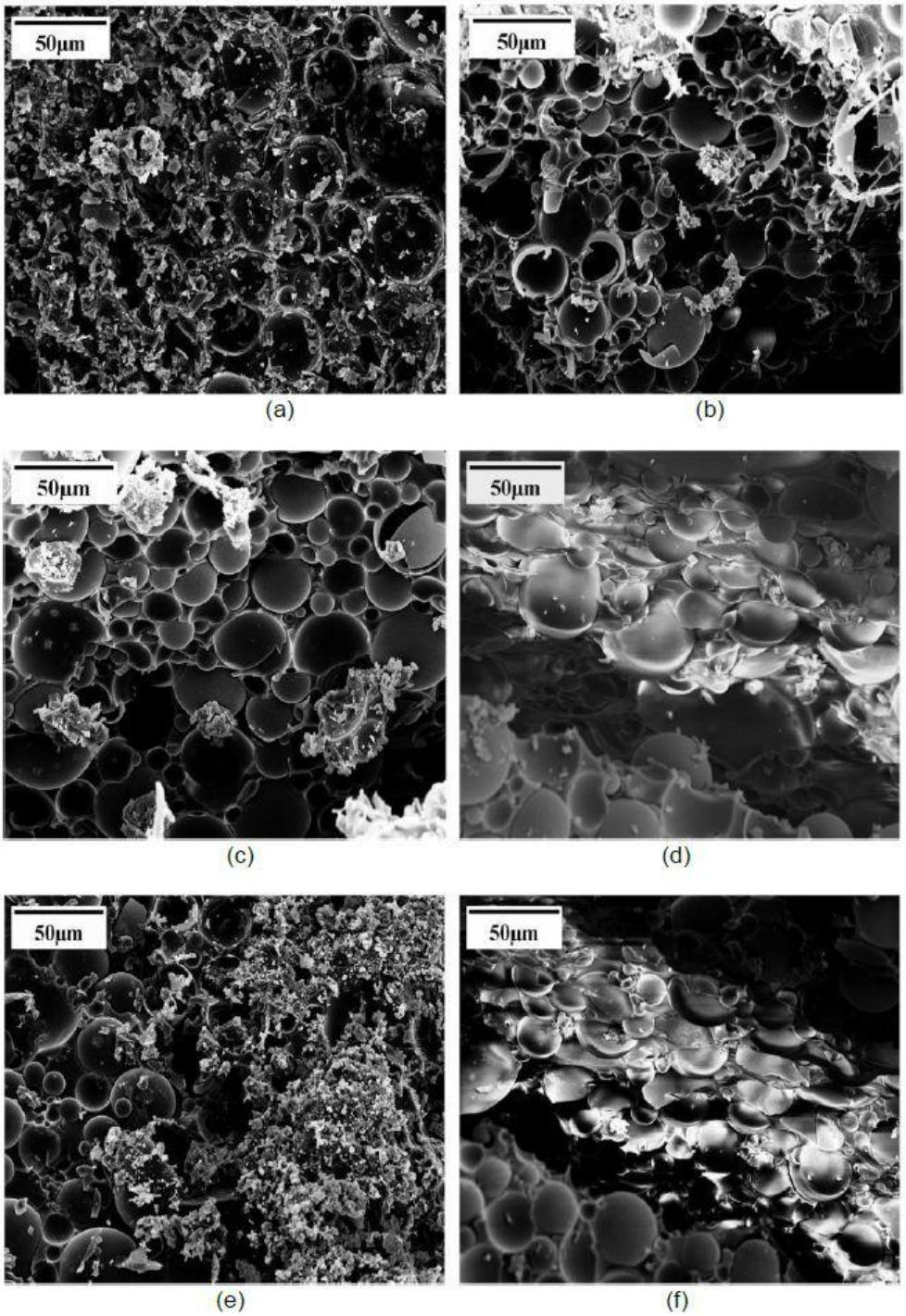

Figure 24 (a) SEM image of S22 and S32 densification at interface in K46-S38-S32-S22
(b) Microballoons behavior inside the crack of S32 layer in K46-S38-S32-S22
(c) Microballoons behavior inside the crack of S38 layer in K46-S38-S32-S22
(d) Microballoons behavior inside the crack of K46 layer in K46-S38-S32-S22
(e) Densification at S22 and K46 microballoon layers interface in K46-S22-S22-K46
(f) Microballoons behavior inside the crack of K46 layer in K46-S22-S22-K46

5.2 Edge- Wise Compression

Five specimens from each IFGSF configuration are tested under edge-wise compression. Stress-strain curves from edge-wise testing of IFGSFs are shown in Figure 25. The variation in stress-strain curves from similar IFGSF configurations is found to be very small (Figure 25). From Figure 25, it is evident that the peak strengths of S32-S38-S38-S32 and S38-S32-S32-S38 IFGSFs are attained in the range of 4.5% to 5% strain. Further, stress values fall down sharply until 7% strain. Also from Figure 25, the peak strengths of S22-K46-K46-S22, K46-S22-S22-K46 and K46-S38-S32-S22 IFGSFs are attained at the range of 4% to 4.5% strains and further follow a sudden drop in stress until to 6% strain. The sudden drop in stress values of five IFGSF configurations is caused by the propagation of vertical crack in S38 and K46 microballoons layers in corresponding IFGSF structures. Furthermore, the stress-strain behavior from edge-wise compression studies of all IFGSFs show a downward trend until 10% to 12% strain after the sudden drop in stress value. The stress plateau extension is large due to higher densification of low density layers.

The edge-wise compressive modulus, strength and energy absorption values are calculated from Figure 25 and are tabulated in Table 7. Compressive modulus is calculated from the slope of the stress-strain plots. The energy absorption is calculated by using trapezoidal area calculation method. Stress-strain curves from edge-wise compression testing of IFGSFs are compared with stress-strain curves of plain foams having similar density and are shown in Figure 26. From Figure 26 and Table 7, it is observed that the compressive strength, energy absorption and modulus values of IFGSFs are higher compared to that of plain syntactic foams.

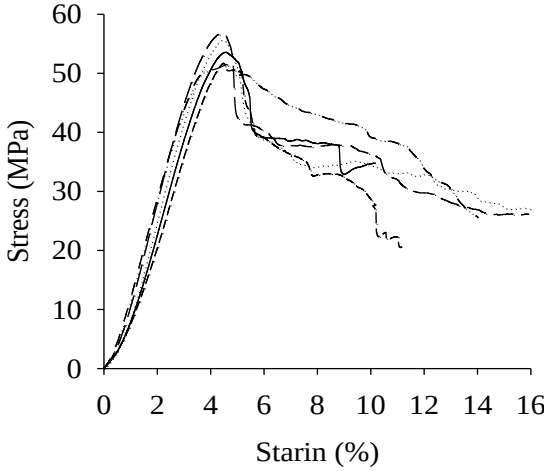

(a) S22-K46-K46-S22 IFGSF structure

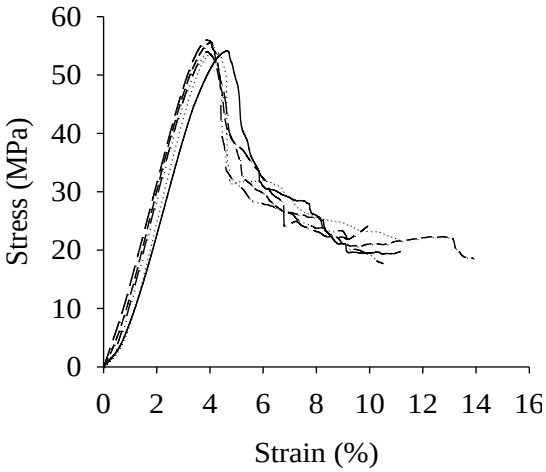

(b) K46-S22-S22-K46 IFGSF structure

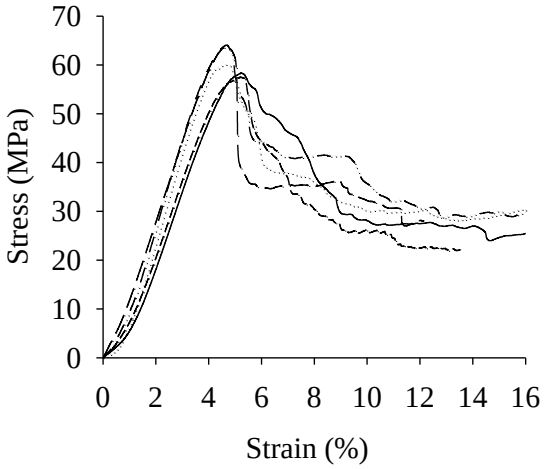

(c) S32-S38-S38-S32 IFGSF structure

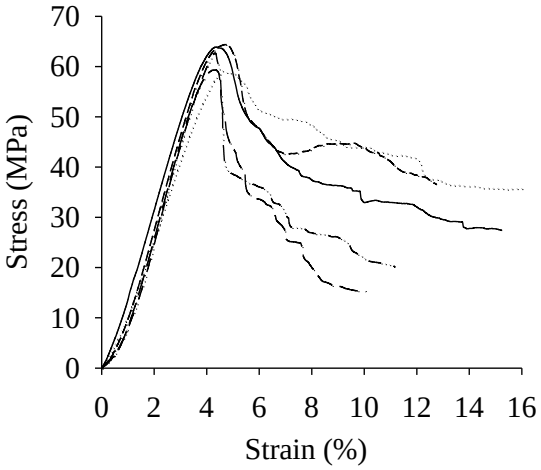

(d) S38-S32-S32-S38 IFGSF structure

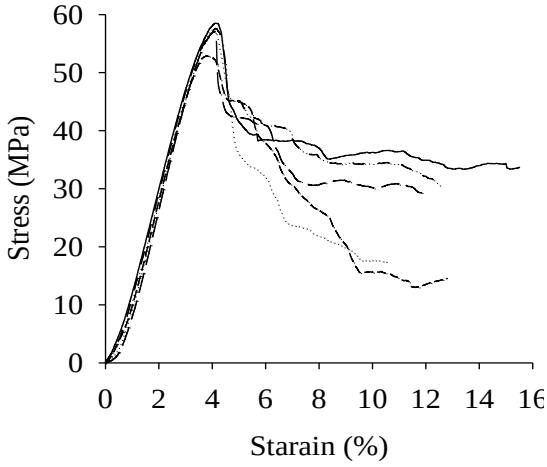

(e) K46-S38-S32-S22 IFGSF structure

Figure 25 IFGSF configurations stress-strain curves repeatability

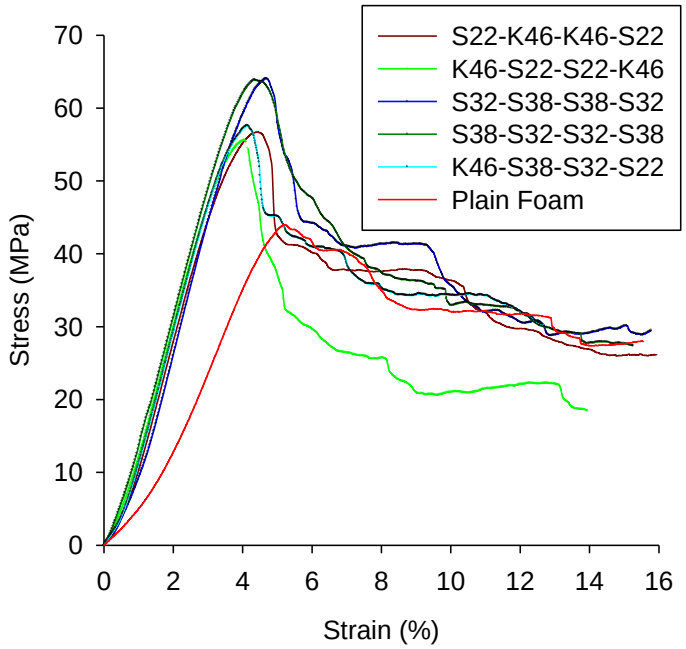

Figure 26 Stress- Strain plots comparison of IFGSF structures and plain foams

Table 7 Edge-wise compressive properties of IFGSF specimens

Type of IFGSF Specimen	**Compressive yield strength (MPa)**	**Compressive Modulus (MPa)**	**Energy Absorption (MPa-mm/mm)**
S22-K46-K46-S22	55.11±2.5	1842±80	3.42±0.3
K46-S22-S22-K46	54.72±1.0	1826±61	2.93±0.2
S32-S38-S38-S32	61.19±2.6	1918±60	3.70±0.2
S38-S32-S32-S38	61.90±2.5	1930±80	3.80±0.3
K46-S38-S32-S22	57.01±1.6	1920±50	3.45±0.2
Plain Foams	44.18±2.4	1181±40	2.85±0.3

The edge-wise compressive yield strength value of plain syntactic foams with similar density to that of IFGSF is found to be 44 MPa. Compared to plain syntactic foams, the compressive yield strengths of S22-K46-K46-S22 and K46-S22-S22-K46 IFGSFs (55 MPa), S32-S38-S38-S32 and S38-S32-S32-S38 IFGSFs (61 MPa) and K46-S38-S32-S22 IFGSF (57 MPa) are found to increase by 25%, 40%, and 30%, respectively. The high yield strengths of

IFGSF structures is due to the high strength contribution by stiffer layers in the configuration. It is evident that stiffer layers (high density layers) have higher yield strength and modulus values compared to low density layers. Even though the stress value of IFGSF structure reaches above the yield strength of individual low density layers, the stress value in the graph continues its increment due to the compressive resistance force applied by the stiffer layers. The stress values increase until the vertical crack is developed in the IFGSF structure.

Compared to plain syntactic foams (2.85 MPa-mm/mm), the energy absorption values of S22-K46-K46-S22 IFGSF (3.42 MPa-mm/mm), S32-S38-S38-S32 and S38-S32-S32-S38 IFGSFs (3.8 MPa-mm/mm) and K46-S38-S32-S22 IFGSF (3.45 MPa-mm/mm) have increased by 20%, 33%, and 21%, respectively (Table 7). This increment in energy absorption is due to the high yield strength contribution by the high density layers while the low density layers help the whole IFGSF structure to extend its stress-plateau region. This is a typical characteristic of high energy absorbing materials. However, the K46-S22-S22-K46 IFGSF configuration does not show significant improvement in energy absorption compared to plain foams due to its structural instability. This instability is due to the failure of individual stiffer layers caused by the high shear and secondary tensile stresses in the structure. The K46 layers peel out due to high stress concentrations caused by the shear and secondary tensile stresses. The steep drop in stress values of K46-S22-S22-K46 IFGSF graph is also shown in Figure 26. Also, it is found that the edge-wise compressive modulus of IFGSF structures is superior compared to plain syntactic foams due to the high strength of stiffer layers.

In order to show the layer sequencing effect on the edge-wise compression properties, IFGSFs with different layer sequencing are compared to one another. From Figure 26 and Table 7, it is observed that the yield strength, modulus and energy absorption values of S32-S38-S38-

S32 and S38-S32-S32-S38 IFGSF configurations are high compared to S22-K46-K46-S22, K46-S22-S22-K46 and K46-S38-S32-S22 IFGSF configurations. The compressive properties of the IFGSF configurations with S32 as the weakest layer (S32-S38-S38-S32 and S38-S32-S32-S38 IFGSFs) are superior compared to the configurations with S22 as the weakest layer in all other IFGSF configurations used in this study. This is due to the higher strength and modulus of S32 microballoons compared to S22 microballoons. Also the density differences in between S32 and S38 are low compared to S22 and K46 microballoons. Hence, the S32-S38-S38-S32 and S38-S32-S32-S38 IFGSFs have more uniform structure compared to all other IFGSFs used in this study. Although the edge-wise properties are mainly dependent on the stiffer layer, due to the effect of secondary tensile stresses in lateral direction, the yield strength of K46 microballoons layer in S22-K46-K46-S22, K46-S22-S22-K46 and K46-S38-S32-S22 IFGSF structures is reduced. The secondary tensile stresses effect increases with an increase in strength of the microballoon. The uniformity and less tensile stress effect on S38 layers compared to K46 layers make S32-S38-S38-S32 and S38-S32-S32-S38 IFGSFs superior compared to all other IFGSFs used in this study.

From Table 7, it can be observed that the energy absorption values of S38-S32-S32-S38 and S32-S38-S38-S32 configurations are similar to each other. However, the energy absorption values of S22-K46-K46-S22 and K46-S22-S22-K46 IFGSF configurations are found to be different. This difference in trends of energy absorption values is due to the radius ratio (η) difference of microballoons. Comparing the radius ratio (η) difference between IFGSF configurations with S32 and S38 microballoons and S22 and K46 microballoons, it is evident that the radius ratio difference between K46 and S22 microballoons is more compared to S32 and S38 microballoons. This difference in radius ratio (η) also causes the structural non-

uniformity. In addition, the energy absorption of S22-K46-K46-S22 configuration is high compared to its counter configuration. This is due to the partial structural instability of K46-S22-S22-K46 IFGSF structure. This instability of the structure is caused by peeling out of individual stiffer layers caused by higher secondary tensile stresses. Also, the stiffer layers weaker resistance to compression result in high stress values drop in K46-S22-S22-K46 IFGSF compared to its counterpart, thereby ultimately reducing the overall energy absorption of the K46-S22-S22-K46 IFGSF structure. Thus, it is evident that the layer sequencing has effect on the edge-wise compression properties of IFGSF structures.

Figure 27(a) - Figure 27(e) show the edge-wise crack propagation behavior of all IFGSF configurations used in this study. The overall crack propagation trend in all IFGSF configurations is in a similar fashion to that of plain foams. Even though the low density layer is the weakest layer in the structure, vertical splitting of the high density layer is predominant in edge-wise IFGSF failure. Vertical splitting is preceded by the initiation of wedge shaped cracks. Initiation of wedge shape cracks is due to shear stresses from the corners and the secondary tensile stresses in the lateral direction.

Figure 27(b) - Figure 27(c) show the edge-wise crack propagation behavior in IFGSF configurations with S22 and K46 microballoons. From Figure 27(b), it can be observed that the shear cracks are developed from the corners due to the direct compressive stress and secondary tensile stresses on individual layers. The secondary tensile stresses effect is more when the difference in densification between low density and high density microballoons layers is more. These shear cracks grow in an inclined manner and form a wedge shaped crack. Shear cracks meet at a point and act as a stress riser. The secondary tensile stresses and the high stress

concentration caused by the shear cracks lead to vertical crack development in the stiffer layer. At the same time, cracks also propagate through the low density layers due to their low strength.

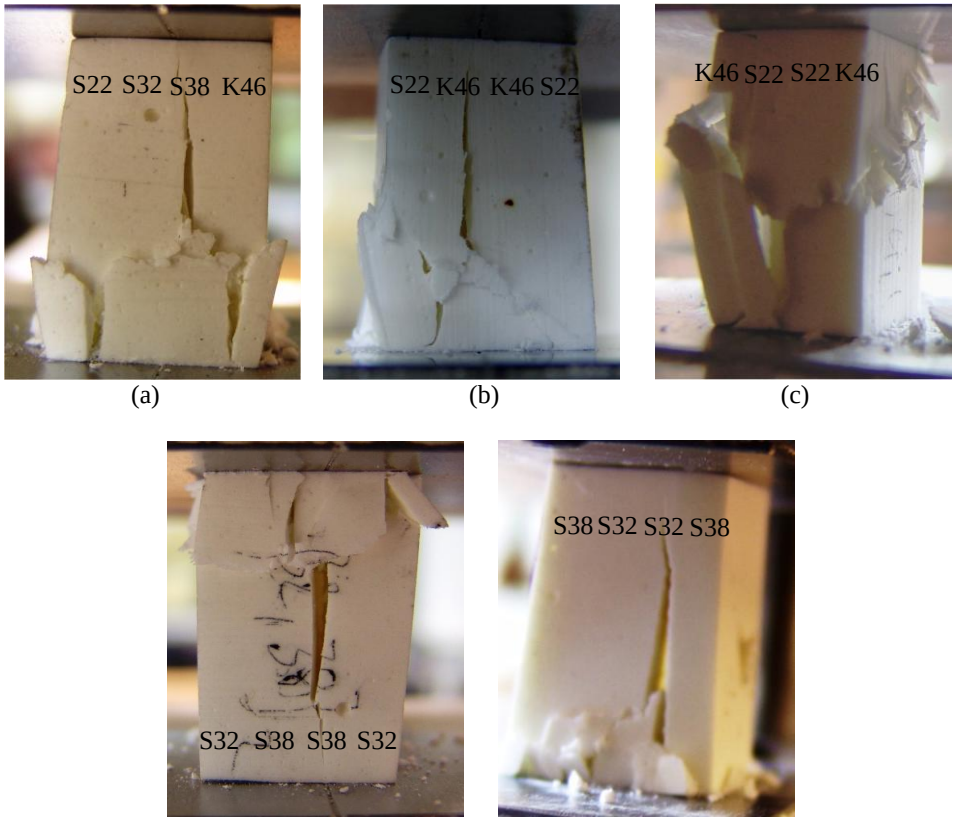

(a) (b) (c)

(d) (e)

Figure 27 Edge-wise compression crack propagation behavior (a) K46-S38-S32-S22 IFGSF crack propagation (b) S22-K46-K46-S22 IFGSF crack propagation (c) K46-S22-S22-K46 IFGSF crack propagation (d) S32-S38-S38-S32 IFGSF crack propagation (e) S38-S32-S32-S38 IFGSF crack propagation

From Figure 27(c), it can be observed that the K46 layer is peeling out due to the partial structural instability of the IFGSF structure caused by high secondary tensile stresses effect on individual K46 layer. The partial structural instability of IFGSF with low density layers at the center causes the reduction in stress value than its counter IFGSF configuration. The lower stress values ultimately reduce the energy absorption. This lower energy absorption and higher

stress values drop in stress-strain curve can also be observed in Figure 26 and Table 7. In case of higher density difference between microballoons, the edge-wise compressive properties and crack propagation of IFGSF structures depend on layer sequencing.

Figure 27(d) - Figure 27(e) show the edge-wise crack propagation behavior in S32-S38-S38-S32 and S38-S32-S32-S38 IFGSF configurations. Even in these IFGSF configurations, crack propagation behavior is similar to that of IFGSF configurations with S22 and K46 microballoons. The vertical splitting of the stiffer layer is preceded by the shear and secondary tensile stresses. The layer sequencing effect on crack propagation behavior of IFGSF with S32 and S38 microballoons is less compared to IFGSFs with K46 and S22 microballoons. However, both IFGSF configurations have same energy absorption capacity.

5.3 Impact Testing

Three samples from each IFGSF configuration are tested at impact velocities of 1m/s, 2m/s and 3m/s on Instron Dynatup-8250 impact machine. The contact force histories for a period of impact on S22-K46-K46-S22 IFGSF sample at varying impact energies are depicted in Figure 28–Figure 30. The contact force is defined as the load that is exerted on the sample during impact while the tup is in contact with the sample. From Figure 28-Figure 30, it can be observed that the contact force history for S22-K46-K46-S22 configuration at impact velocities of 1 m/s and 2 m/s is a smooth curve resembling characteristics of no damage or permanent deformation from this impact [76]. Similar contact force histories at impact velocities of 1 m/s, and 2 m/s are observed for other IFGSF configurations in this study. However, the contact force history at impact velocity of 3 m/s is not a smooth curve as shown in Figure 30. This contact force curve is a resemblance of extended damage on the sample. Similar behavior at impact velocity of 3 m/s is observed for all the other IFGSF configurations used in this study.

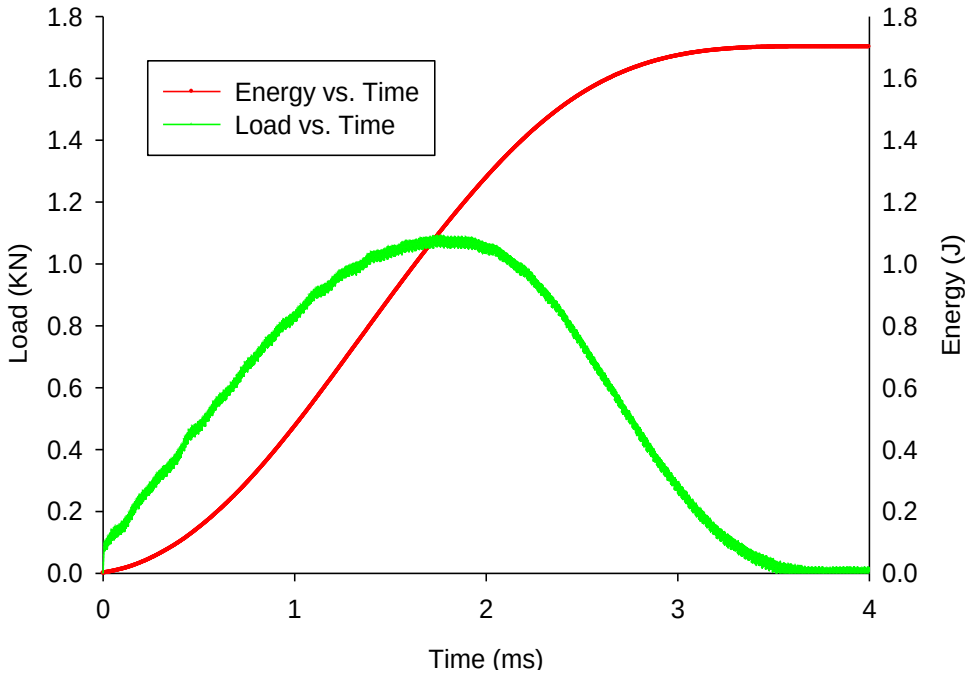

Figure 28 S22-K46-K46-S22 IFGSF configuration Load vs. time and Energy vs. time plot at 1 m/s velocity, equivalent to 1.7 J energy

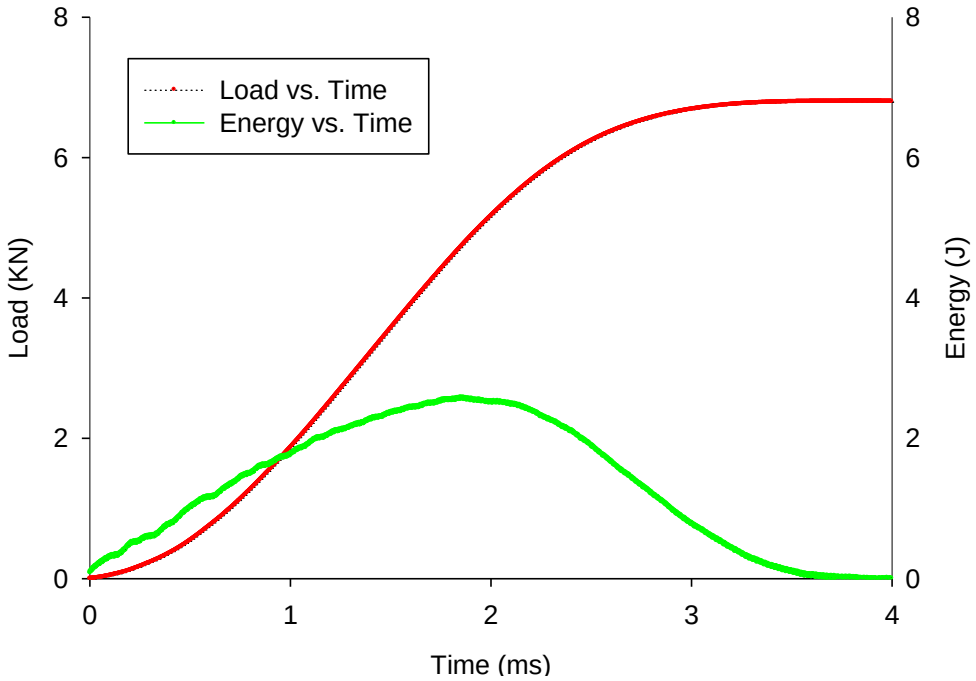

Figure 29 S22-K46-K46-S22 IFGSF configuration Load vs. time and Energy vs. time plot at 2 m/s velocity, equivalent to 6.8 J energy

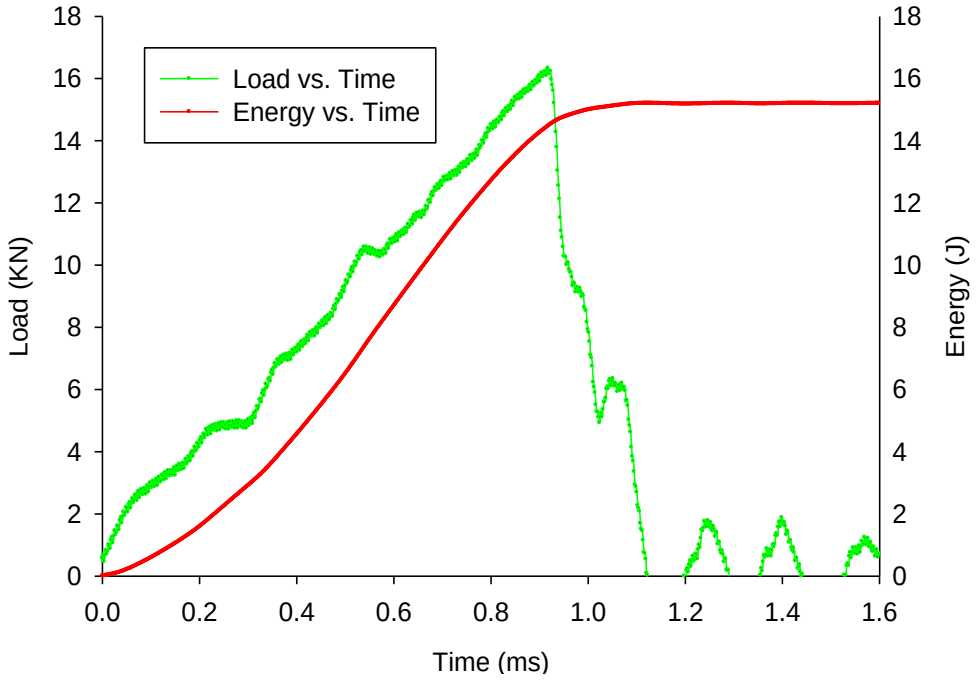

Figure 30 S22-K46-K46-S22 IFGSF configuration Load vs. time and Energy vs. time plot at 3 m/s velocity, equivalent to 15.3 J energy

The maximum contact force or maximum load for different IFGSF configurations at different impact energies are shown in Table 8-Table 10. From Table 8- Table 9, it can be observed that the maximum load sustained by different IFGSF configurations at impact energy of 1.7 J is almost similar to each other. Similar trend is observed in maximum load values of IFGSF configurations at impact energy of 6.8 J. This can be attributed to the fact that at impact velocities of 1 m/s and 2m/s, IFGSF configurations are subjected to localized damage close to the point of impact as shown in Figure 31-Figure 32. However, K46-S22-S22-K46 IFGSF have marginally higher maximum load values compared to its counter configuration at 1 m/s impact velocity. Similar behavior is also observed at 2 m/s impact velocity. These differences in maximum loads in IFGSFs with S22 and K46 microballoons, at 1 m/s and 2m/s, are shown in Figure 33- Figure 34. This is due to the stiffer K46 layer sustaining more loads compared to S22 layer. Comparing IFGSF configurations with S32 and S38 microballoons, it is observed that

S38-S32-S32-S38 and S32-S38-S38-S32 IFGSFs sustain similar maximum load. This behavior is due to smaller radius ratio (η) differences between S32 and S38 microballoons. Therefore, the effect of layer orientation on the impact resistance is not observed in IFGSF configuration with less radius ratio variations. .

Table 8 Impacted with 1.7 J (Total Energy)

Configuration	Velocity (m/s)	Initiation Energy (J)	Propagation Energy (J)	Maximum Load (KN)
S22-K46-K46-S22	1	1.08±0.01	0.61±0.01	1.10±0.01
K46-S22-S22-K46	1	1.09±0.05	0.61±0.05	1.16±0.01
S32-S38-S38-S32	1	1.05±0.02	0.64±0.02	1.25±0.06
S38-S32-S32-S38	1	1.08±0.05	0.61±0.05	1.21±0.05
K46-S38-S32-S22	1	1.07±0.04	0.63±0.04	1.10±0.02

Table 9 Impacted with 6.8 J (Total Energy)

Configuration	Velocity (m/s)	Initiation Energy (J)	Propagation Energy (J)	Maximum Load KN
S22-K46-K46-S22	2	4.75±0.07	2.04±0.07	2.70±0.01
K46-S22-S22-K46	2	4.64±0.14	2.18±0.14	3.03±0.01
S32-S38-S38-S32	2	4.61±0.16	2.19±0.16	2.98±0.10
S38-S32-S32-S38	2	4.72±0.10	2.08±0.10	2.95±0.01
K46-S38-S32-S22	2	5.21±0.06	1.60±0.06	3.01±0.02

Figure 31 Impact damage of S22-K46-K46-S22 IFGSF at energy 1.7 J

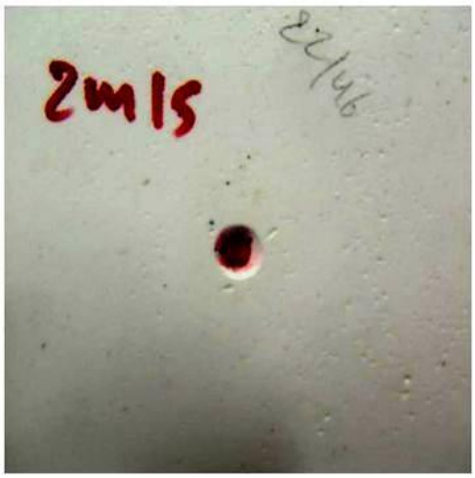

Figure 32 Impact damage of S22-K46-K46-S22 IFGSF at energy 6.8 J

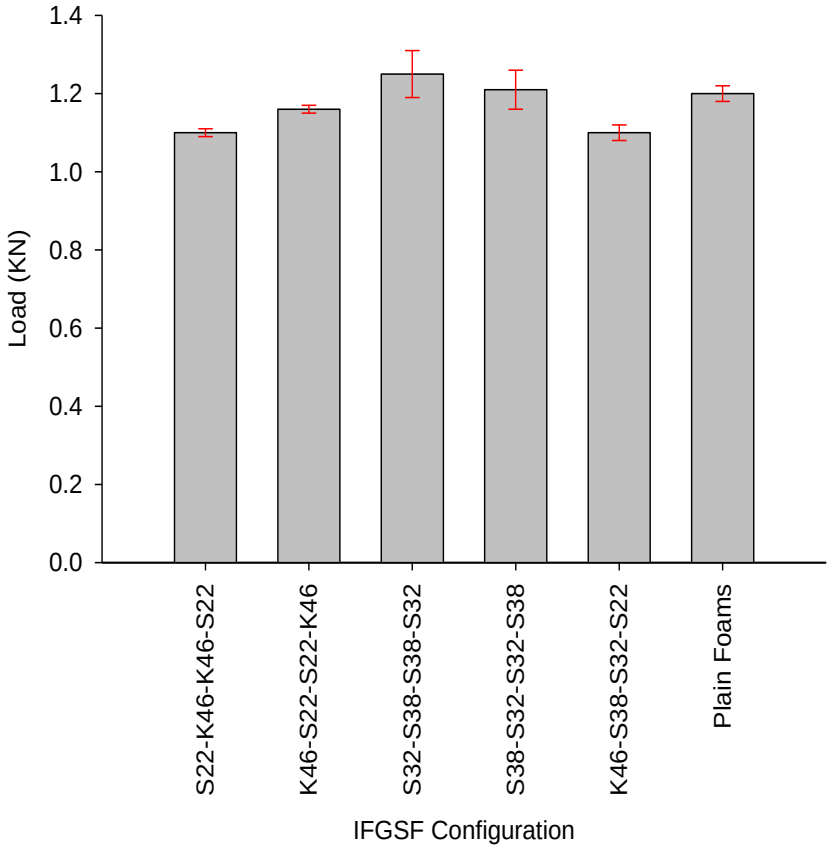

Figure 33 IFGSF configurations and plain foams maximum load values bar graph at 1 m/s impact velocity, equivalent to 1.7 J

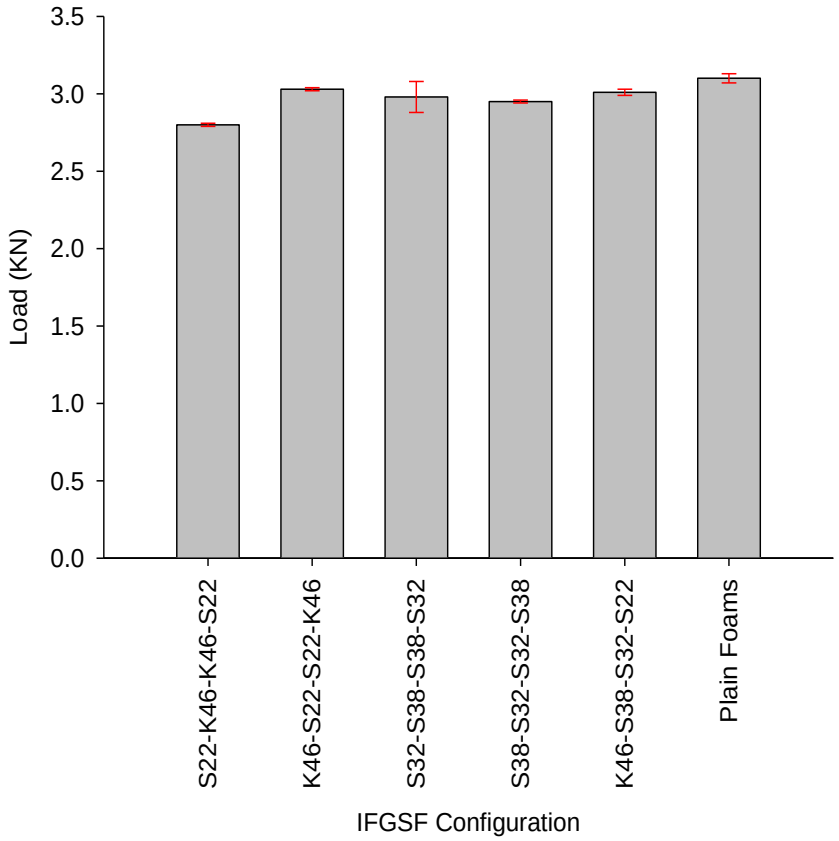

Figure 34 IFGSF configurations and plain foams maximum load values bar graph at 2 m/s impact velocity, equivalent to 6.8 J

The maximum load values of IFGSFs at 1 m/s, 2m/s and 3m/s have compared with plain foams having similar density. It is found that the maximum load values of plain foams and IFGSFs are similar (Figure 33- Figure 35). Further, the maximum contact force at 3m/s impact velocity shows variation with IFGSF configuration. From Table 10 and Figure 35, it can be observed that the maximum contact force for IFGSF configurations with K46 and S22 microballoons is more than the maximum contact force for IFGSF configuration with S32 and S38 microballoons. This difference in maximum contact force between IFGSF configurations is due to the effect of stiffer layer (K46) on impact properties. At impact energy of 15.3 J (3 m/s impact velocity), IFGSF configurations are subjected to global damage (Figure 36) rather than local damage as in the case of impact damage at 1m/s and 2 m/s. Therefore, the stiffer layer in

the configuration affects the maximum contact force. It is evident that the maximum load increases with an increase in density of microballoons. In addition, the maximum contact force for S32-S38-S38-S32 and S38-S32-S32-S38 configuration is similar to each other. However, the maximum contact force for S22-K46-K46-S22 and K46-S22-S22-K46 IFGSF configurations are different from each other. This difference in trend in maximum contact force is due to the difference in radius ratios (η) of the IFGSF configuration. Higher radius ratio (η) microballoons at outer layers sustain maximum load compared to lower radius ratio (η) microballoons due to their stiffer nature. The radius ratio (η) difference between S32 and S38 microballoons is less compared to K46 and S22 microballoons.

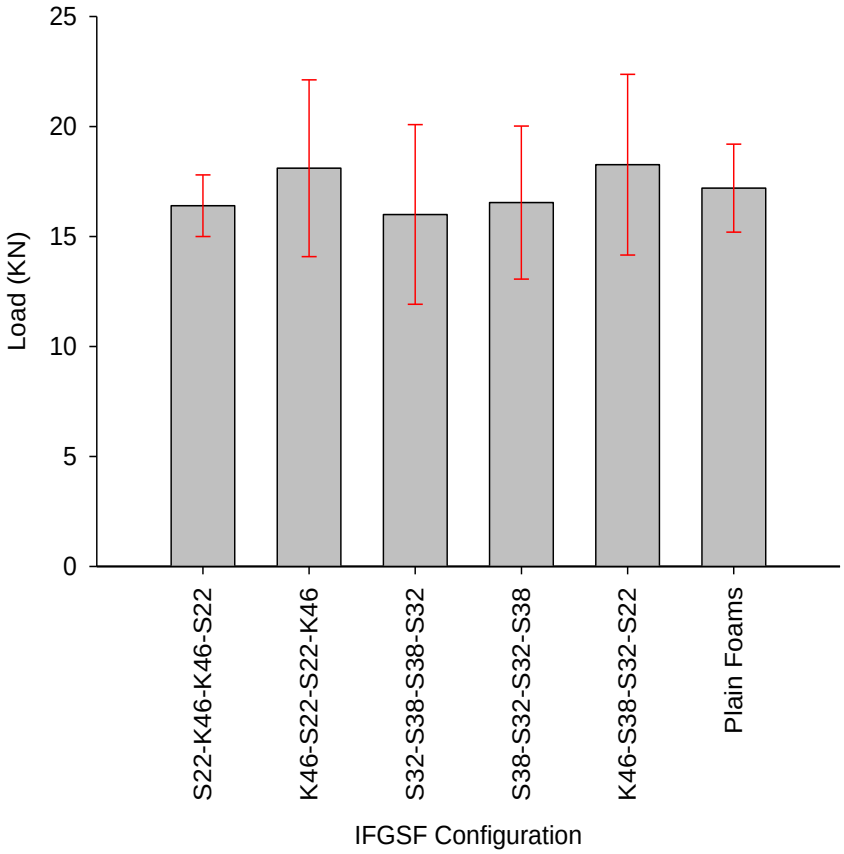

Figure 35 IFGSF configurations and plain foams maximum load values bar graph at 3 m/s impact velocity, equivalent to 15.3 J

Table 10 Impacted with 15.3 J (Total energy)

Configuration	Velocity (m/s)	Initiation Energy (J)	Propagation Energy (J)	Maximum Load (KN)
S22-K46-K46-S22	3	14.40±0.10	0.80±0.11	16.40±1.40
K46-S22-S22-K46	3	14.60±0.30	0.60±0.14	18.10±4.02
S32-S38-S38-S32	3	14.80±0.10	0.26±0.12	14.12±4.08
S38-S32-S32-S38	3	14.60±0.05	0.55±0.01	14.10±3.48
K46-S38-S32-S22	3	14.80±0.20	0.46±0.01	18.26±5.11

Figure 36 Impact damage of S22- K46-K46-S22 IFGSF at energy 15.3 J

Initiation and propagation energy values of IFGSF configurations are also shown in Tables 8-Table 10. From Tables 8-Table 9, it can be observed that the initiation energies of IFGSF configurations at impact energy of 1.7 J are similar to each other. Propagation energies of IFGSF configurations at 1.7 J are also similar to each other. Similar trend is observed for IFGSF configurations at impact energy of 6.8 J. The initiation and propagation energies comparison of IFGSFs and plain foams at 1m/s and 2m/s are shown in Figure 37- Figure 38. Even though localized damage is observed in all IFGSF configurations at impact energies of 1.7 and 6.8 J, energy is transferred from one layer to the other during impact. Hence, initiation and propagation energies are not affected by layer sequencing. Also the plain foams with similar density having same initiation and propagation energies compared to plain foams. From Table

10 and Figure 39, it can be observed that the initiation energies of IFGSF configurations at impact energy of 15.3 J are similar to each other. However, considerable variation in propagation energies is observed at impact energy of 15.3 J. This difference in trend between initiation and propagation energy can be attributed to the global damage on the IFGSF configuration at impact energy of 15.3 J. Due to this reason, cracks initiate at the same energy in different configurations but propagate depending on the IFGSF configuration. Hence, the propagation energy values of IFGSF configurations at impact energy of 15.3 J are dependent on the properties of syntactic foam layers. Thus the layer sequencing does not show any effect on initiation and propagation energies.

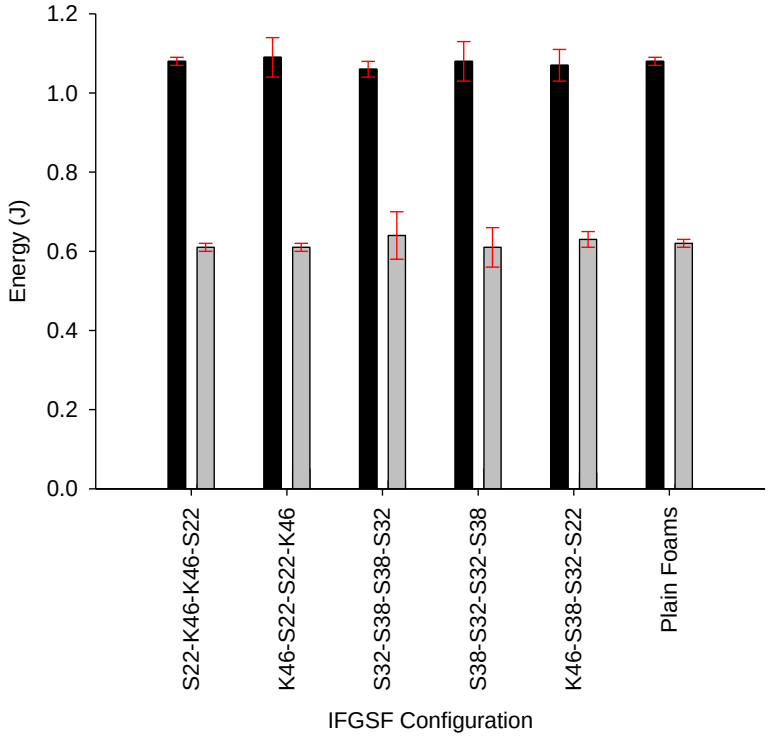

Figure 37 Initiation and propagation energies comparison of plain foams and IFGSF configurations having similar density at 1m/s impact velocity

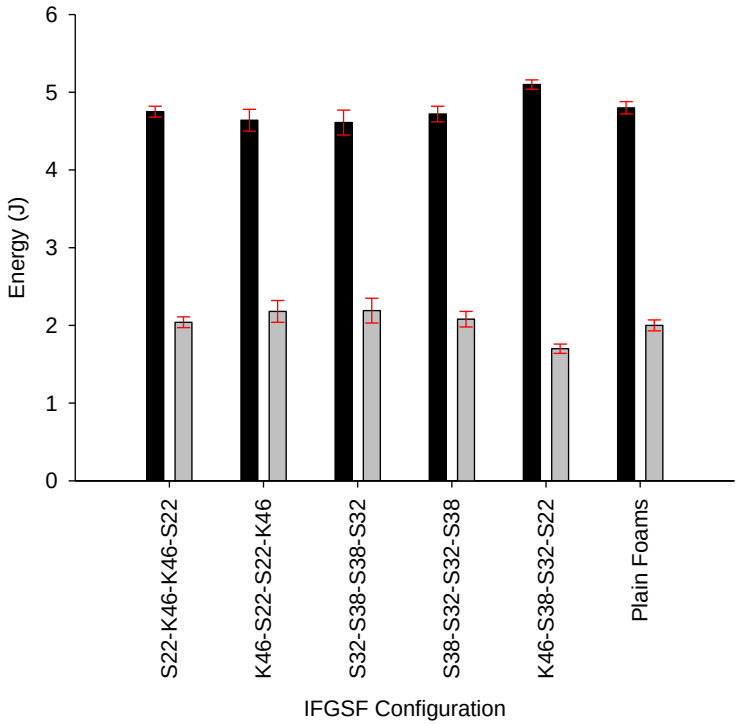

Figure 38 Initiation and propagation energies comparison of plain foams and IFGSF configurations having similar density at 2 m/s impact velocity

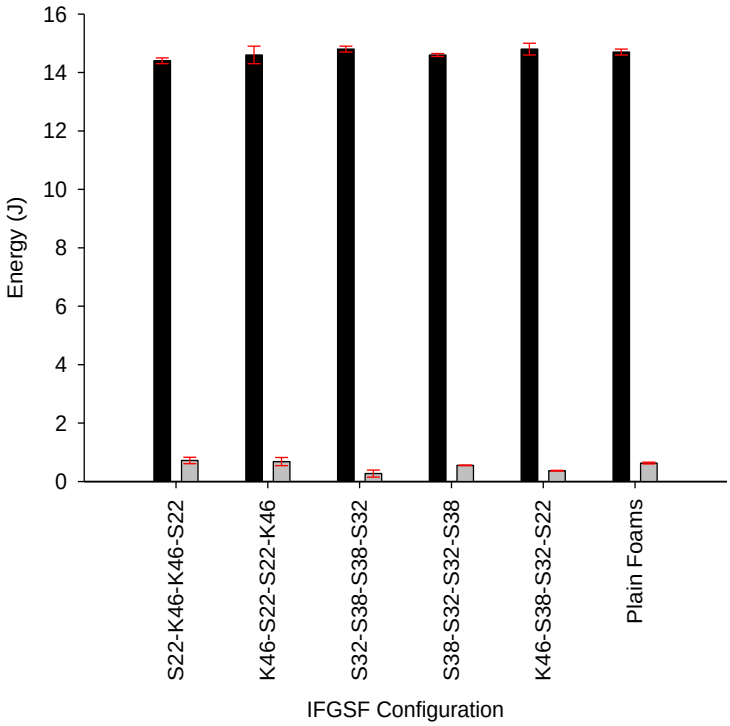

Figure 39 Initiation and propagation energies comparison of plain foams and IFGSF configurations having similar density at 2 m/s impact velocity

CHAPTER 6. CONCLUSIONS AND FUTURE WORK

6.1 Conclusions

.Five different layer sequencing IFGSF configurations are fabricated using layer over layer integration technique. Four of the IFGSF configurations are symmetric over the central plane while the fifth configuration is an integration of all four microballoons incorporated syntactic foam layers. The volume fraction of microballoons is maintained constant at 60%. The layer over layer integrated technique has developed to fabricate the gradient syntactic foams.

In order to understand the compressive behavior in IFGSFs, five specimens of each of the configurations are tested in quasi-static flat-wise and edge-wise compression using MTS-810 servo-hydraulic machine. The flat-wise compression results are compared with plain syntactic foams and with adhesively bonded FGSF having similar density. It is found that the stress-strain plateau in IFGSF structures extends from 8% to 60% strain in contrast to an extension from 10% to 20% for plain syntactic foams with similar density. Hence, an increase in energy absorption for IFGSF structures is obtained. This increase in energy absorption can be attributed to the high energy absorption by low density layers. On contrary, the high density layers in IFGSF contribute more to the strength of the IFGSF structure. Compared to the adhesively bonded FGSF, the IFGSFs with similar layer sequencing show an improvement of 50% and 75% in compressive yield strength and energy absorption, respectively. In order to show the layer sequencing effect on the compressive properties of gradient structures, results from different configurations are compared to one another. It is found that S32-S38-S38-S32 and S38-S32-S32-S38 IFGSF configurations exhibited higher compressive properties compared to all other IFGSF configurations used in this study. This is due to the dependency of the flat-wise compression properties on the weakest layer of gradient structures. As S32 layer is superior

compared to S22 microballoon layer, configurations with S32 microballoons show better compressive properties. Although the compressive yield strength values are found to be similar, symmetric IFGSF configurations with denser microballoons in the central layer (S32-S38-S38-S32 and S22-K46-K46-S22) show enhanced energy absorption compared to their counterparts. The densification and initiation of crack is found to always take place in the weakest layer of the IFGSF configuration.

The edge-wise IFGSF structures compressive properties are compared with plain foams having similar density. Additionally, IFGSFs with different layer sequencing are compared to one another. Compared to plain syntactic foams, the compressive yield strengths of S22-K46-K46-S22 and K46-S22-S22-K46 IFGSFs, S32-S38-S38-S32 and S38-S32-S32-S38 IFGSFs and K46-S38-S32-S22 IFGSF are found to increase by 25%, 40%, and 30%, respectively. Compared to plain syntactic foams, the energy absorption values of S22-K46-K46-S22 IFGSF, S32-S38-S38-S32 and S38-S32-S32-S38 IFGSFs and K46-S38-S32-S22 IFGSF are found to increase by 20%, 33%, and 21%, respectively. This increase in energy absorption can be attributed to the high energy absorption by low density layers. The edge-wise IFGSF properties mainly depend on the stiffer layer in that configuration. Vertical splitting of the denser layer is a predominant factor in the failure of edge-wise IFGSF structures. Vertical splitting in the denser layer is due to the wedge shaped crack caused by the shear stresses and secondary tensile stresses.

In addition to compression analysis, IFGSF configurations are tested for low velocity impact properties at 1 m/s, 2 m/s and 3 m/s velocities on Dynatup 8250 impact testing machine. The impact testing results of all the IFGSF configurations are compared to one another. The initiation energy and propagation energy values of five IFGSF configurations at 1.7 J, 6.8 J and 15.3 J are found to be same. This is due to localized damage at low impact velocities. Hence the

effect of layer sequencing is not observed in initiation and propagation energies. Thus, it is concluded that similar density syntactic foam structures have similar impact properties at lower velocities. The maximum load values of K46-S22-S22-K46 IFGSF configuration have higher maximum load value compared to its counter configuration. The maximum load values of IFGSFs with higher density variations in microballoon layers change with layer sequencing.

6.2 Future Work

In order to verify accuracy in experimental data, FEM analysis is to be performed. Further, ultrasonic analysis need to be performed to understand the damage behavior in impacted samples. Variation in impact damage with variation in impact velocity is to be characterized using ultrasonic imaging.

REFERENCES

1) Engineered Materials Handbook Desk Edition, "ASM International," www.asm-intl.org. (Members only online access).

2) H. Katz, and J. V. Milewski, "Handbook of reinforcements for plastics," Van Nostrand Reinhold Co., New York, 1987.

3) M. Guy, Genin, and V. Birman, "Micromechanics and structural response of functionally graded, particulate-matrix, fiber-reinforced composites," International Journal of Solids and Structures, Vol. 46, pp: 2136-2150.

4) Engineering Materials Handbook, "ASTM International," www.astm.org. (Members only can access).

5) K. Ashida, "Syntactic foams. In: Handbook of Plastic Foams: Types, Properties, Manufacture and Applications," Edited by Landrock AH. New Jersey: Noyes Publications, 1995. pp. 147-163.

6) N. Gupta, B. S. Brar and E. Woldesenbet, "Effect of Filler Addition on the Compressive Compressive and Impact Properties of Glass Fibre Reinforced Epoxy", Bulletin of Materials Science, Vol. 2, pp. 219-223, 2001.

7) K. Ashida and A. H. Landrock, Handbook of Plastic Foams: Types, Properties, Manufacture and Applications, Noyes Publications, ,pp. 147-163, 1995.

8) J. R. M. d'Almeida, "An Analysis of the Effect of the Diameters of Glass Microspheres on the Mechanical Behavior of Glass-Microsphere/Epoxy-Matrix Composites", Composites Science and Technology Composites Composites Science and Technology, Vo. 59, pp. 2087-2091, 1999.

9) E. Woldesenbet, N. Gupta, and H. D. Jerro, "Effect of Microballoon Radius Ratio on Syntactic Foam Core Sandwich Composites", Journal of Sandwich Structures and Materials, Vol. 7, pp. 95-111, 2005.

10) Liying Zhang, and J. Ma., "Processing and characterization of syntactic carbon foams containing hollow carbon microspheres," Carbon vol. 47,1451-1456, 2009.

11) N. Gupta, E. Woldesenbet, Kishore and S, Sankaran, "Response of Syntactic Foam Core Sandwich Structured Composites to Three-Point Bending", Journal of Sandwich Structures and Materials, Vol. 4, pp. 249-272, 2002.

12) R. A. Malloy and J. A. Hudson, In: International Encyclopedia of Composites, edited by M. Lee, VCH,1990.

13) L. Bardella, and F. Genna, "On the elastic behavior or syntactic foams," Int J Solids Stru; 38:7235-7260, 2001.

14) N. Gupta, E, Kishore, E. Woldesenbet and S. Sankaran, "Studies on Compressive Failure Features in Syntactic Foam Material" Journal of Materials Science, Vol. 36, No. 18, pp. 485-4491, 2001.

15) F. A Shutov, "Syntactic Polymer Foams, Advances in Polymer Science, Vol 73, pp. 63-123, 1986.

16) N. Gupta, and W. Ricci, "Comparison of compressive properties of layered syntactic foams having gradient in microballoon volume fraction and wall thickness," Materials Science and Engineering A, 427: 331–342, 2006.

17) N. Gupta, E. Woldesenbet and P. Mensah, "Compression Properties of Syntactic Foams: Effect of Cenosphere Radius Ratio and Specimen Aspect Ratio", Composites: Part A, Vol. 35, pp. 103-111, 2004.

18) Gupta, N., and Woldesenbet, E., "Experimental investigation on the effect of cenosphere radius ratio on the flatwise compressive properties of syntactic foams," Composites Part A: Applied Science and Manufacturing, 35(1):103-111, 2004.

19) E.M. Woutersona, F.Y.C. Boeya, S.-C. Wongb, L. Chenc and X. Hu "Nano-toughening versus micro-toughening of polymer syntactic foams," Composites Science and Technology Volume 67, Issue 14, Pages 2924-2933, November 2007.

20) R. Maharsia, N. Gupta, and H. D. Jerro, "Investigation of flexural strength properties of rubber and nanoclay reinforced hybrid syntactic foams," Materials Science and Engineering, Vol. 417, pp: 249-258

21) Y. J. Huang, Vaikhanski, Lev and Steven R. Nutt "3D long fiber-reinforced syntactic foam based on hollow polymeric microspheres," Composites Part A: Applied Science and Manufacturing, Vol. 37, pp:488- 496

22) Y. Zheng, and R. Ning, "Effects of Nanoparticles SiO2 on the Performance of Nanocomposites", Materials Letters, Vol. 57, pp. 2940-2944, 2003.

23) M.V. Alonsoa, M. L. Auada and S. Nutt., "Short-fiber-reinforced epoxy foams," Composites Part A: Applied Science and Manufacturing, Vol.37, pp:1952-1960, 2005.

24) Jessica Agde Tjernlund, E. Kristofer Gamstedta and Peter Gudmundson, "Length-scale effects on damage development in tensile loading of glass-sphere filled epoxy" International Journal of Solids and Structures Volume 43, Issue 24, PP: 7337-7357, 2006.

25) J. Leidner, and T. Woodhams, "The strength of polymeric composites containing spherical fillers," J Appl. Polym. Sci. 18, 1639-1654, 1974.

26) A. J Hodge, "Materials and processes laboratory composite materials characterization," NASA Technical Report: NASA/TM 2000; 210252, 1991.

27) M. Suits, “Analysis of a functionally graded particulate composite under flexural loading conditions,” NASA Technical Report: NASA/TM—1999–209148, 1999.

28) N. Gupta, and E. Woldesenbet, “Hygrothermal studies on syntactic foams and compressive strength determination,” Composite Structures, 61(4): 311-320, 2003.

29) C. S. Karthikeyan, Kishore, and S. Sankaran, “Effect of absorption in aqueous and hygrothermal media on the compressive properties of glass fiber reinforced syntactic foam, “ J. Reinf. Plast. Comp., 20(11): 982-993, 2001.

30) N. Gupta, Kishore, E. Woldesenbet, and S. Sankaran, “Studies on compressive failure features in syntactic foam material,” Journal of Material Science, 36(18): 4485-4491, 2001.

31) N. Gupta, C. S. Karthikeyan, S. Sankaran, and Kishore, ‘Correlation of Processing Methodology to the Physical and Mechanical Properties of Syntactic Foams With and Without Fibers’, Materials Characterization 43, 4, 271-277, 1999.

32) P. Bunn, and J. T. Mottram, ‘Manufacture and Compression Properties of Syntactic Foams’, Composites 24, 7, 565-571, 1993.

33) N. Gupta, Kishore, E. Woldesenbet, and S. Sankaran, ‘Studies on compressive failure features in syntactic foam material’, Journal of Materials Science 36, 18, 4485-4491, 2001.

34) W. H. Lin and M. H. Jen, “Manufacturing and Mechanical Properties of Glass Bubbles/Epoxy Particulate Composites” Journal of Composite Materials, Vol. 32, No. 15. pp. 1356-1390, 1998.

35) N. Gupta, and E. Woldesenbet, “Microballoon Wall Thickness Effects on Properties of Syntactic Foams”, Journal of Cellular Plastics, Vol. 40, pp. 461-480, 2004.

36) H. S. Kim and P. Plubrai, “Manufacturing and Failure Mechanisms of Syntactic Foam Under Compression”, Composites: Part A. Vol. 35, pp. 1009-1015, 2004.

37) N. Gupta and R. Nagony, “Tensile Properties of Glass Microballoon-Epoxy Resin Syntactic Foams”, Journal of Applied Polymer Science, Vol. 102, pp. 1254-1261, 2006.

38) Kishore, Ravi Shankar , S. Sankaran, 2005, “Gradient syntactic foams: Tensile strength, modulus and fractographic features,” Materials Science and Engineering A, 412:153–158.

39) H. S. Kim, H. H. Oh, J. Appl. Polym. Sci., 76 1324-1328, 2000.

40) H. S. Kim, M. A. Khamis, Compos. Part A-Appl S., 32 1311-1317, 2001.

41) M. Todo,, K. Takahashi, and K. Higuchi "Impact fracture behavior of glass bubbles filled epoxy resins," In Proceedings of ASC 16th Annual Conference, Paper # 059, Blacksburg, VA, Sept. 9-12, 2001.

42) S. S. Cheon, J. H. Choib and D. G. Lee, "Development of the Composite Bumper Beam for Passenger Cars", Composite Structures, Vol. 32, pp. 491-499, 1995.

43) S. S. Cheon, D. G. Lee and K. S. Jeon, "Composite Side-Door Impact Beams for Passenger Cars", Composite Structures, Vol. 38, No. 1-4, pp. 229-239, 1997.

44) N. Gupta, Kishore and S. Sankaran, "On the Characterization of Syntactic Foam Core Sandwich Composites for Compressive Properties", Journal of Reinforced Plastics and Composites, Vol. 18, No. 14, pp. 1347-1357, 1999.

45) H. Kim, and M. Kamis, "Fracture and impact behaviors of hollow micro-sphere/epoxy composites", Composites Part A: Applied Science and Manufacturing, Volume32 (9), 1311-1317, 2001.

46) E. Woldesenbet, "Low Velocity Impact Properties of Nanoparticulate Syntactic Foams", Materials Science and Engineering A, Vol. 496, No. 1-2, pp. 217-222, 2008.

47) E. Woldesenbet, P. Mylavarapu and N. Sankella, "Response of Nanoclay Syntactic Foam Sandwich Structured Composites to Low Velocity impact," proceedings of Journal of Sandwich Structures and Materials.

48) N. Gupta, Kishore and S. Sankaran, "On the Characterization of Syntactic Foam Core Sandwich Composites for Compressive Properties", Journal of Reinforced Plastics and Composites, Vol. 18, No. 14, pp. 1347-1357, 1999.

49) Rizzi. E. Papa and A. Corigliano, "Mechanical behavior of a Syntactic Foam: Experiments and Modeling", International Journal of Solids and Structures, Vol. 37, pp. 5773-5794, 2000.

50) G. Li, V. Muthyala, "Impact characterization of sandwich structures with an integrated orthogrid stiffened syntactic foam core", Composites Science and Technology, Volume 68 (9), 2078-2084, 2008.

51) V. Chakka, "Quasi-static and Impact Characterization of Sandwich Structures with an Iso-Grid Stiffened Syntactic Foam Core," Dept of mechanical Engineering, Masters Thesis, 2008.

52) N. Gupta and E. Woldesenbet, "Characterization of Flexural Properties of Syntactic Foam Core Sandwich Composites and Effect of Density Variation", Journal of Composite Materials, Vol. 39, No. 24, pp. 2197-2212, 2005.

53) B. Song, W. Chen, T. Yanagita and D. J. Frew, "Confinement Effects on the Dynamic Compressive Properties of an Epoxy Syntactic Foam", Composite Structures, Vol. 67, pp. 279-287, 2005.

54) S. V. Thiruppukuzhi and C. T. Sun, “Testing and Modeling High Strain Rate Behavior of Polymeric Composites”, Composites: Part B, Vol. 29B, pp. 535-546. 1998.

55) S Peter, E Woldesenbet, “Nanoclay syntactic foam composites—High strain rate properties,” Materials Science and Engineering: A Volume 494, Issues 1-2, 25 PP 179-187, 2008.

56) E. Woldesenbet, N. Gupta, and A. Jadhav, “Effects of density and strain rate on properties of syntactic foams,” . Journal of Materials Science, 40(15):4009-4017, 2005.

57) S. C. M. Yen and C. T. Liu, “Effect of Strain Rate on the Near Crack Tip Behavior of a Particulate Composite”, Internation Journal of Damage Mechanics, Vol. 9, pp. 352-377, 2000.

58) B. C. Ray, S. T. Hasan, and D. W. Clegg,” Evaluation of Defects in FRP Composites by NDT Techniques”, Journal of Reinforced Plastics and composites, Volume 26 (12), 1187-1192, 2007.

59) P. Mylavarapu and E. Woldesenbet, “Characterization of syntactic foams- an Ultrasonic Approch,” Journal of Cellular Plastics, Vol. 44, No. 3, 203-222, 2008.

60) N. Gupta and R. Maharsia, “Enhancement of Energy Absorption in Syntactic Foams by Nanoclay Incorporation for Sandwich Core Applications”, Applied Composite Materials, Vol. 12, pp 247-261, 2005.

61) R. Maharsia and H. D. Jerro, “Enhancing Tensile Strength and Toughness in Syntactic Foams Through Nanoclay Reinforcement”, Materials Science and Engineering A, Vol. 454-455, pp. 416-422, 2007.

62) Y. Zheng, Y. Zheng and R. Ning, “Effects of Nanoparticles SiO2 on the Performance of Nanocomposites”, Materials Letters, Vol. 57, pp. 2940-2944, 2003.

63) G. Li, and J. Nji, “Development of Rubberized Syntactic Foam,” Composite Part A: Applied Science and Manufacturing, Volume 38 (6), 1483-1492, 2007.

64) V. Parameswaran, and A. Shukla,“Processing and characterization of a model functionally gradient material”, Journal of Materials Science, 35(1): 21-29, 2000.

65) V. Parameswaran, and A. Shukla,, “Near-tip out of plane displacement fields for dynamic crack propagation in functionally graded materials”, Mechanics Research Communications, 29(5):397-405, 2002.

66) M. A. El-Hadek,, and. H. V. Tippur, “Dynamic fracture parameters and constraint effects in functionally graded syntactic epoxy foams”, International Journal of Solids and Structures, 40(8): 1885-1906, 2003.

67) N. Gupta, “A functionally graded syntactic foam material for high energy absorption,” Materials Letters, 61(4-5):979-982, 2007.

68) Lucas F M da Silvaa, R. D. Adams, “Techniques to reduce the peel stresses in adhesive joints with composites”, International Journal of Adhesion and Adhesives, 27:227-235, 2007.

69) Technical Data Sheet. DOW Liquid Epoxy Resins.

70) Product Information. D.E.R 332 Liquid Epoxy Resin. DOW Chemical Company.

71) Technical Bulletin, C12-C14 Glycidyl Ether, Erisys GE-8, CVC Specialty Chemicals.

72) Product Information. D.E.H 24 Epoxy Curing Agent. DOW Chemical Company.

73) ASTM C 271 – 94., “Standard test method for density of sandwich core materials,” ASTM International, PA, USA.

74) ASTM C 365/C 365M-05., “Standard test method for density of sandwich core materials,” ASTM International, PA, USA.

75) ASTM D 695-96., “Standard test method for density of sandwich core materials,” ASTM International, PA, USA.

76) B. D. Agarwal, and J. Broutl, “ Analysis and performance of fiber composites,” J. wiley, second edition, 1990.

VITA

Kanakaji Chittineni was born in Perecherla, Guntur, Andhra Pradesh, India, in the year 1984. He completed his schooling from M. P. U. P School and S. G. V. R High School, Guntur, India, and Mechanical Engineering Diploma education from M. B. T. S Govt. Polytechnic College, Guntur, India. His interest in mechanics and their applications made him to join Mechanical Engineering Department at QISCET, Ongole, Andhra Pradesh, India and earned a Bachelor of Engineering in the year 2006. He then decided to pursue higher education and enrolled in the master's program in Louisiana State University, Baton Rouge, United States of America, in Fall 2007. He will be graduating in August 2009 with Master of Science in Mechanical Engineering.